8

Underwater Acoustic Communications

David Brady
James C. Preisig

Much of the development of the preceding chapters is applicable to a broad range of wireless networks, although there is a strong emphasis on radio-frequency (RF) systems and their applications. And while underwater acoustic channels and systems share many features with their RF counterparts, there are also important differences. In this chapter, we describe the special characteristics of underwater acoustic channels and show how they impact system design.

The underwater acoustic channel (UAC) is quite possibly nature's most unforgiving wireless communication medium. Multipath delay spreads exceed 60 ms for horizontal medium-range channels, and frequency responses may exhibit deep nulls. Fading processes may be fast or slow, frequency selective or frequency nonselective, depending on the direction of propagation and conditions of the water column. Battery and mission lifetimes restrict the transmitter powers of practical modems to 30W. High-frequency absorption losses and low-frequency ship noise confine the transmission bandwidth to less then 40 kHz for medium-range shallow-water applications. The UAC is a broadcast channel, and the aggregate bandwidth must be shared by an asynchronous group of noncooperating

users. The low propagation velocity of sound in water (1500 m/s) translates wave or modest platform motion to significant Doppler compression and permits the use of a slowly time-varying channel model only if phase and synchronization tracking are given special attention.

Underwater communication has been used since the beginning of the 20th century to permit a data link between the surface and the water column [20].[1] Today underwater acoustic telemetry is used to communicate between untethered platforms, such as underwater vehicles (UV) and data logging stations. Manned or unmanned oceanographic exploration, ocean monitoring, and the offshore oil industry all rely on underwater acoustic telemetry.

This chapter presents an overview of the state of underwater acoustic communications and the role of signal processing in this field. We begin with the development of an appropriate channel model. We describe the relationship between environmental conditions and the characteristics of the channel model, then we analyze the impact of these characteristics on the communications problem. We then turn our attention to digital modulation and signal processing techniques that facilitate demodulation: adaptive equalization, estimation, and detection in sparse systems, multiuser detection, and multisensor detection. We present adaptive techniques that are especially suited for the UAC to reduce convergence time, tracking error, or computational complexity. The chapter also highlights current problems in this active research area and reviews approaches to their solutions.

8.1 The Underwater Acoustic Channel

From the communications perspective, the underwater acoustic channel poses many challenges to the realization of reliable, high-rate communications. In this section, we summarize many of the salient physical characteristics of the channel and their effects on the communications problem. The section begins with a discussion of the ray model for acoustic propagation, its dependence on the speed of propagation of sound in the ocean, and the dominant mechanisms for sound speed variability in the ocean. Then, we address the bandwidth constraints imposed by the absorption and spreading of sound in the ocean, the sources of noise in the ocean, and their effects on achievable signal to noise ratios. Finally, we discuss the dominating influence of both time-invariant and time-varying multipath propagation and relate these effects to the input/output response and statistical characterization

[1]However, the possibilities of underwater communication were envisioned by Leonardo da Vinci as early as 1490: "If you cause your ship to stop, and place the head of a long tube in the water and place the outer extremity to your ear, you will hear ships at a great distance from you." (See [1].)

of the communications channel. Excellent material covering the general topic of sound propagation in the ocean is contained in [2, 3].

8.1.1 The Ray Propagation Model

In most conditions, sound waves at middle and high frequencies (> 5 kHz) can be reasonably modeled as propagating along paths or rays through the ocean. A good rule of thumb is that this model is valid when the spatial scale of the inhomogeneities in the ocean is larger than the wavelength of the sound. Since the speed of sound is approximately 1500 m/s in the ocean, the wavelength in this region is less than one-third of a meter. In a homogeneous environment, the rays' paths would follow straight lines radiating from the source. However, the sound speed structure of the ocean is highly variable, both spatially and temporally. In accordance with Snell's Law, the spatial variability induces a bending of the rays referred to as *refraction*. Consider a simplified, two-dimensional model for the ocean, shown in Figure 8.1, in which the sound speed c is a function of depth z.

In this case, the path of a refracted ray in this environment is described by the pair of differential equations

$$\frac{d\theta}{dx} = c(z)^{-1} \frac{dc(z)}{dz} \tag{8.1}$$

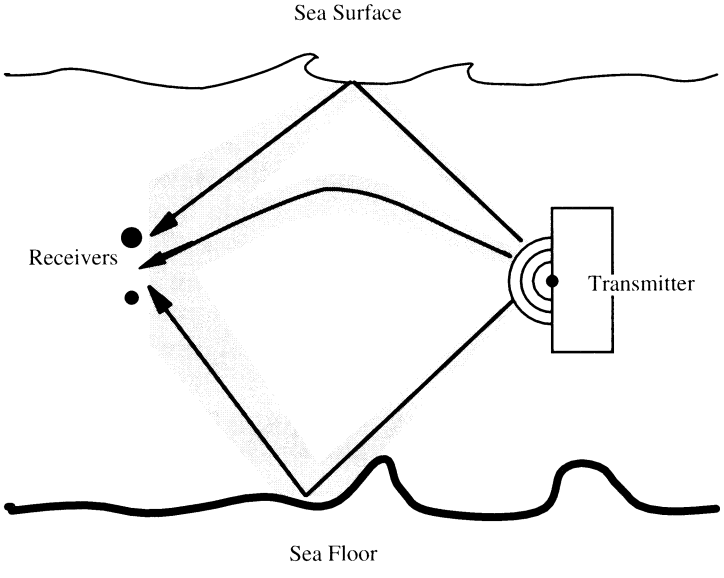

Figure 8.1 The ray model for acoustic propagation.

and

$$\frac{dz}{dx} = -\tan(\theta(x)). \tag{8.2}$$

Here, x denotes the horizontal distance from the source, $z(x)$ denotes the depth of the ray at that range, and $\theta(x)$ denotes the angle of the path with respect to the horizontal ($\theta(x) < 0$ indicates a ray pointed downward). In an environment in which the speed of sounds varies in all three physical dimensions (x, y, and z), the ray paths refract horizontally as well as vertically. However, the spatial gradient of the speed of sound tends to be much smaller in the horizontal than in the vertical, so the horizontal refraction is usually much smaller than the vertical refraction.

In addition to refraction within the water column, rays experience reflection from the sea surface and sea floor. The nature and strength of the reflections or scattering depend primarily on the amplitude and spatial scale of the roughness of the water/air or water/bottom interface and the density, sound speed, and absorption properties of the bottom material. Accounting for both the refraction of rays as described by Snell's Law and the reflection of rays at the sea surface and sea floor, the sound propagates along many paths from a source to a receiver, as shown by the solid lines in Figure 8.1. The nature and effects of this multipath propagation are discussed more fully in Section 8.1.4.

8.1.2 Sources of Sound Speed Variability

The spatial and temporal variability of the speed of sound in water is a result of the inhomogeneity of the physical properties of the water. A reasonable approximation of the sound speed in sea water is given by [2]

$$\begin{aligned} c(T, S, z) = {} & 1449.2 + 4.6T - 0.055T^2 + 0.00029T^3 \\ & + (1.34 - 0.01T)(S - 35) + 0.016z. \end{aligned} \tag{8.3}$$

Here, c is the sound speed in meters/second, T is the water temperature in degrees Celsius, S is the salinity in parts per thousand, and z is the depth in meters of the point at which the sound speed is evaluated. The dependence of sound speed on depth is due to the dependence of sound speed on the hydrostatic pressure. The functional dependence of the speed of sound on environmental conditions yields different sound speed characteristics in different environments.

In the deep oceans at mid-latitudes, the approximately isosaline water combined with solar heating of the upper portion of the water column yields the characteristic sound velocity profile shown in Figure 8.2. When this type of sound velocity profile is encountered, the refraction of rays towards the region of minimal

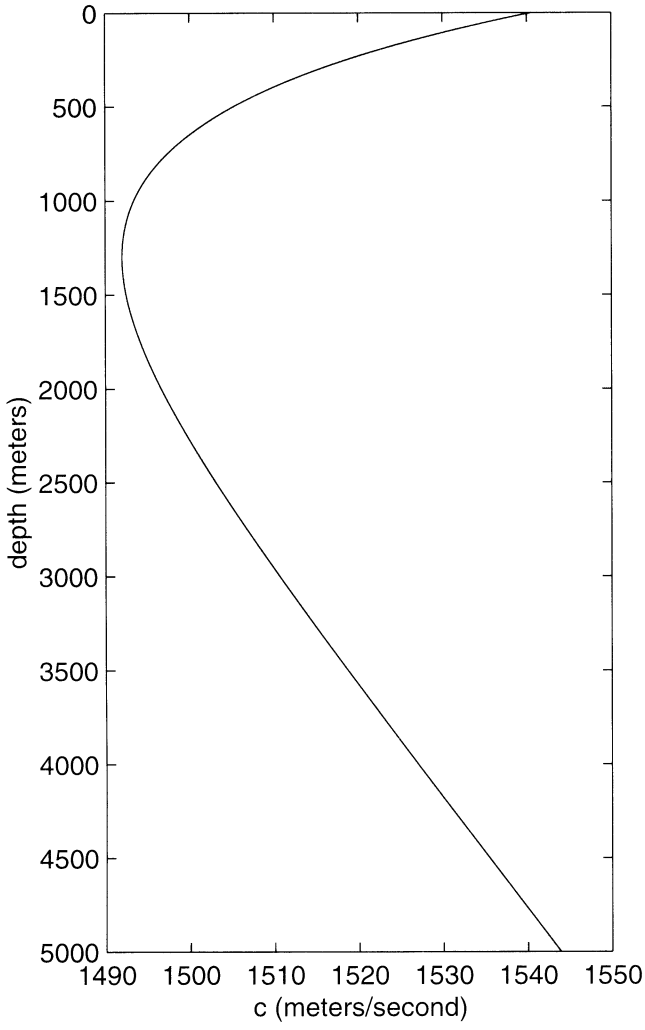

Figure 8.2 Typical deep water sound speed profile.

sound speed creates a natural waveguide in which rays are trapped. This region is referred to as the *sound channel,* or *SOFAR channel.*

In shallow waters, a greater variety of sound speed conditions is often encountered. Following the passage of a storm when the entire water column has been well mixed or in the winter months when solar heating is minimal, the sound speed is nearly constant with depth. At other times, solar heating, the presence of less saline water flowing from rivers and bays, and the tidally driven mixing of this water with oceanic water masses yield a characteristic sound speed profile, shown in Figure 8.3. With no mid-water sound channel present, sound propagating in shallow water experiences a greater extent of interaction with the sea surface and

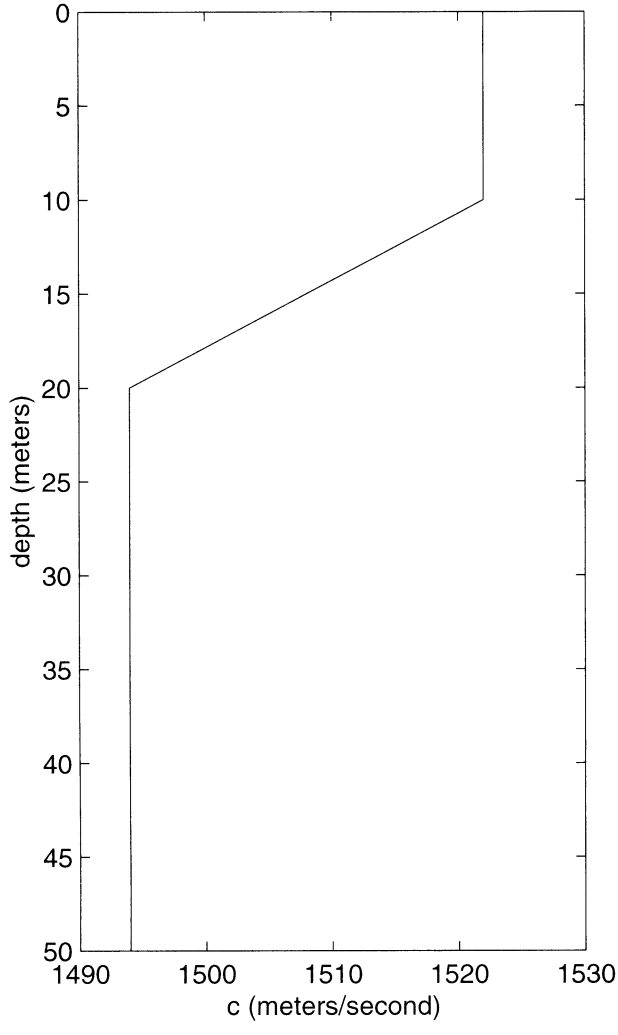

Figure 8.3 Typical shallow water sound speed profile.

sea floor than generally occurs in the deep oceans. In general, this interaction results in higher signal losses and temporal variability.

8.1.3 Signal Losses and Ambient Noise

The signal losses encountered by propagating sound and the ambient noise present in the ocean significantly influence the received signal-to-noise ratio (SNR). The primary mechanisms of signal loss are *spreading loss*, *absorption loss* in both the water and the bottom, and *scattering loss* at the sea surface and sea floor. The

spreading loss associated with the propagation of sound occurs in primarily two types. In regions close to the sound source where the wavefront radiates spherically, the conservation of energy results in an attenuation of the signal energy by a factor of r^{-2}, where r is the range from the source. Further from the source, the vertical propagation of the sound energy reaches the limits imposed by the sea bottom, sea surface, or sound channel. At this point, the wavefront begins to radiate in a cylindrical fashion from the source, and the resulting attenuation of the signal energy is by a factor of r^{-1}.

While the speed of sound and spreading losses are independent of the frequency of the sound, the absorption of sound by the water is highly dependent on frequency. The absorption of sound by the water is the result of the conversion of acoustic energy into heat. A number of physical mechanisms govern this conversion (see [3] for a complete description). Formulas such as Eq. (3.3.6) in [3] are available to compute the attenuation rate of sound due to absorption in sea water. Figure 8.4 shows the attenuation coefficient in dB/kilometer as a function of frequency for sound in sea water at the sea surface with a temperature of 14 degrees Celsius and salinity of 35 parts per thousand. As can be seen, the attenuation coefficient rises rapidly with frequency, effectively limiting the channel bandwidth at all but very short ranges.

Acoustic signals are attenuated by interaction with the sea surface and sea floor. The losses are caused by rough surface scattering at both interfaces and absorption losses within the bottom. When the sea surface is rough, the reflection of the acoustic energy from the surface is not specular but is scattered in a multitude of directions. Most of the energy that is scattered in a direction other than the direction of the receiver is effectively lost. While the sea floor does not perfectly reflect acoustic signals, the reflected signals also contain a mixture of specularly reflected and scattered signals. Once again, the energy in the scattered signal is lost. In addition, since the reflection of energy at the sea floor is incomplete, sound will penetrate into the bottom. The absorption of sound in the bottom is significantly higher than that in the water, resulting in further signal losses.

In the deep oceans, the presence of the sound channel limits the surface and bottom interaction. Sound propagating in the SOFAR channel interacts with neither the sea surface nor sea floor and can travel for long distances with no attenuation other than spreading losses and absorption by the water. Any sound that leaves the sound channel and interacts with the sea surface or sea floor is attenuated quickly and is often ignored at ranges past a few times the water depth. However, in shallow water the lack of a mid-water sound channel makes surface and bottom reflected signals a significant portion of the propagating sound. On all but the calmest of days, the rough characteristic of the sea surface yields nonspecular scattering of the sound. The scattering loss associated with sound interaction with the sea surface

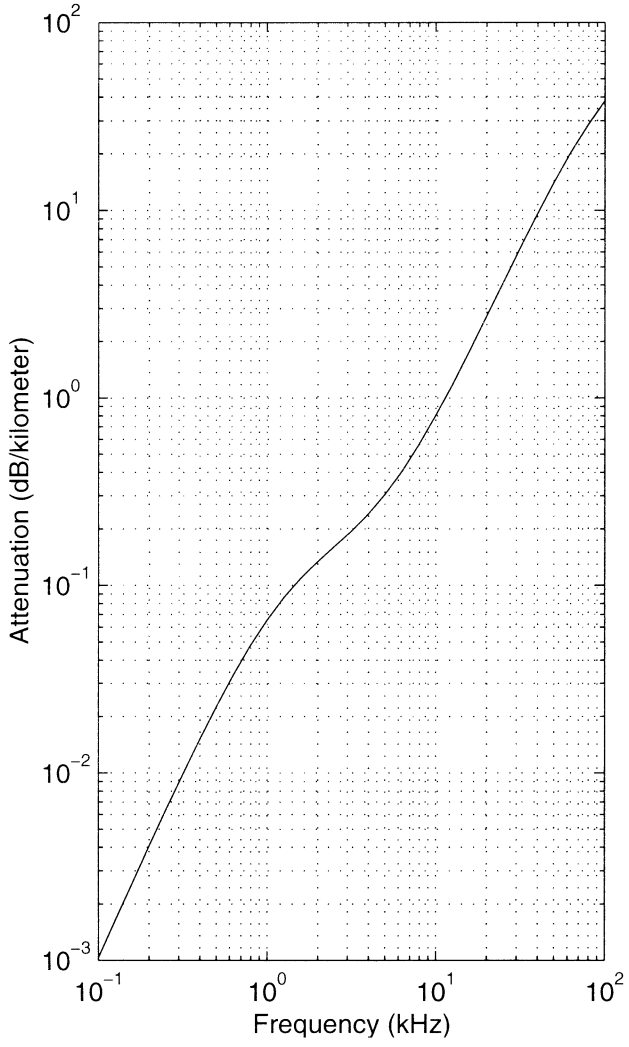

Figure 8.4 Attenuation of sound in sea water.

and the scattering and absorption loss associated with sound interaction with the sea floor conspire to reduce the effective range over which sound will travel in shallow water. Bottom interaction losses are most prevalent in the presence of downward refracting sound speed profiles, such as that shown in Figure 8.3. See [2] for a more complete treatment of these effects.

A second major determinant of the received signal-to-noise ratio is the *ambient noise* present in the ocean. There are many sources of ambient noise in the ocean, including breaking waves, marine life, and passing ships. The nature of the noise depends strongly on its source. Significant noise can be generated by marine

organisms such as whales, fish, and shrimp. In the case of shrimp, the noise is highly impulsive and can severely disrupt the operation of a communications system [4, 5]. Another significant natural source of ambient noise is that generated near the surface of the ocean by breaking waves and rain. Since the generation of breaking waves is primarily driven by the winds, noise generated by these sources is highly dependent on the weather conditions [38]. Man-made sources of noise in the ocean contribute to the ambient noise as well. Predominant among these sources are ships' propulsion machinery. With a large number of possible sources in the ocean, the level of the total ambient noise field can vary widely. In one location over a several-week period, measured noise levels ranging from 90 dB to 120 dB were reported [6].

Ignoring the losses due to surface and bottom interaction, signal fading due to multipath effects, and the effects of shadow zones (regions where rays of sound will not reach), the average signal power at a range r from a narrowband source can be estimated by

$$SL \approx 169 \text{ dB} + 10\log_{10}(P) - \alpha_s r - 20\log_{10}(d/2) - 10\log_{10}(r - d/2). \quad (8.4)$$

Here, SL is the signal level in dB, P is the radiated signal power in watts, α_s is the absorption coefficient in dB/meter, r is the range in meters, and d is the ocean depth in meters. It has been assumed here that the radiating transducer is omnidirectional and that $r > d$. The first two terms account for the radiated power, the third term accounts for absorption loss, the fourth term approximates spherical spreading loss, and the final term approximates cylindrical spreading loss. Assuming a center frequency of 15 kHz, the water conditions used to generate Figure 8.4, a water depth of 50 m, and a radiated power of 20 W, the average signal power as a function or range (in kilometers) is shown in Figure 8.5. Assuming that ambient noise conditions range between 90 dB and 120 dB, as reported above, signal-to-noise levels can be seen to range from 32 dB to 2 dB at 1-km range and 8 dB to -22 dB at 10-km range.

8.1.4 The Multipath Propagation Model

As in the case of RF systems discussed in earlier chapters, multipath propagation is one of the dominant environmental influences on the performance of acoustic communications systems in the ocean. This multipath is usually time-varying, and there are many sources of the temporal fluctuations. These include internal waves (i.e., vertical movement of the inhomogeneous layers of the water mass), internal turbulence, tidal flows, surface waves, and platform motion. Researchers have long attempted to develop a stochastic framework for characterizing and analyzing the effect these fluctuations have on acoustic signals. The seminal work in this

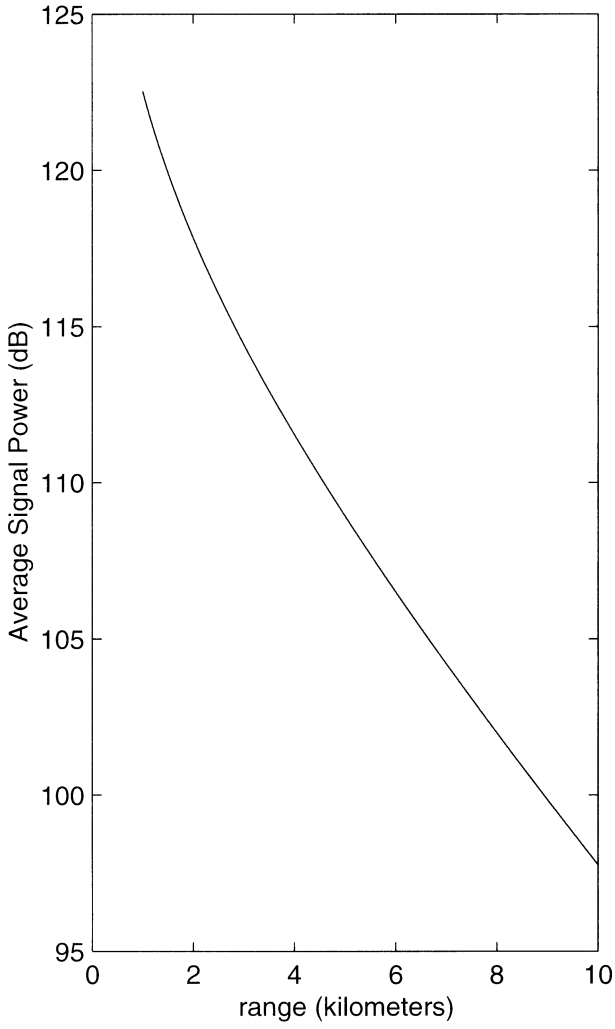

Figure 8.5 Example of signal level vs. range.

area was published in 1979 and reviewed in 1983 [7, 8]. These works concentrate on analyzing the effect of internal waves on acoustic propagation in deep water. However, the paradigm developed therein of decomposing the path followed by sound into micro- and macro-multipath structure serves as a useful starting point for analyzing more general environmental fluctuations. Analyzing these fluctuations in the shallow-water environment continues to be an active area of research. Chapter 10 of [2] also contains a good treatment of the subject. The analysis in [7] and the many derivative publications consider the propagation fluctuations for a propagating monochromatic signal. In Section 8.1.4.1, this method of analysis is detailed. In Section 8.1.4.2, the results from Section 8.1.4.1 are extended to include

wideband signals and yield a description of the fluctuations in the input/output response of the channel.

8.1.4.1 Micro- and Macro-Multipath

The micro- and macro-multipath classification decomposes the acoustic channel into that portion whose characteristics depend on slowly varying and quasi-deterministic properties of the ocean and that portion whose characteristics depend on rapidly varying stochastic properties of the ocean. We begin by representing the spatially and temporally varying sound speed structure of the ocean, using

$$c(\mathbf{z}, t) = c_0(1 + U_0(\mathbf{z}, t) + \mu(\mathbf{z}, t)). \tag{8.5}$$

Here, c_0 represents the nominal sound speed, $\mathbf{z}$ is the spatial position vector, and $U_0(\mathbf{z}, t)$ represents the spatially and temporally variant changes to the index of refraction caused by static or slowly changing environmental factors. Such factors include pressure changes with depth and the variations in water temperature and salinity caused by tidal cycles, daily heating and cooling, seasonal changes, and large-scale geographic variations. The term $\mu(\mathbf{z}, t)$ represents the rapid changes to the index of refraction caused by such sources as internal waves and turbulence.

Suppose a source at a particular location transmits a signal $e^{j\omega t}$, and suppose that signal is received by a sensor at another location. Assume that there are no rapid stochastic fluctuations in the environment (i.e., $\mu(\mathbf{z},t) = 0$), that the sea surface is flat, and that the sea floor has only large-scale features. Here, the terms small and large scale refer to spatial scales that are small or large with respect to the nominal acoustic wavelength, $2\pi c_0/\omega$. Let $\tilde{X}_l(t, \omega)$ be the portion of the received signal that would propagate along the lth ray connecting the source to the receiver. We can express $\tilde{X}_l(t, \omega)$ as

$$\tilde{X}_l(t, \omega) = H_l(t, \omega)e^{j\omega t}, \tag{8.6}$$

where $H_l(t, \omega)$ is a complex-valued function that accounts for the slowly varying phase delay and attenuation of the signal propagating along the lth ray. $H_l(t, \omega)$ depends not only on c_0 and $U_0(\mathbf{z}, t)$ but also on the source and receiver positions and the large-scale bathymetric features of the sea floor. The rays defined under the above assumptions (e.g., the solid lines in Figure 8.1) are referred to as the *macro-multipath structure* of the channel.

If we remove the three aforementioned assumptions, the sound would not necessarily follow the rays defined by the macro-multipath structure. Instead, the sound would be refracted and scattered by the small-scale features represented by $\mu(\mathbf{z}, t)$ and the roughness of the sea surface and sea floor. In this case, the actual path followed by the sound is modeled as staying within a ray tube surrounding the nominal ray. In Figure 8.1, the gray regions represent the ray tubes surrounding each nominal ray. For small-amplitude or large-scale environmental fluctua-

tions, the sound may follow a single perturbed path within a ray tube. As the amplitude of the fluctuations increases and their scale decreases, the single path followed by the sound may split into many micropaths within the ray tube. Thus, the portion of the received signal that propagates within the lth ray tube will be the sum of signals that propagate along the one or more micropaths within the tube. These micropaths constitute the *micro-multipath structure* of the channel. Accounting for the combination of signals propagating along the micropaths within the ray tube, we can express the portion of the received signal that propagates through the lth ray tube as

$$X_l(t, \omega) = \Psi_l(t, \omega)\tilde{X}_l(t, \omega) = \Psi_l(t, \omega)H_l(t, \omega)e^{j\omega t}. \tag{8.7}$$

Here, $\Psi_l(t, \omega)$ accounts for the fluctuations in the received signal due to the micro-multipath structure of the lth ray tube.

Accounting for all of the rays between the source and receiver, the received signal can be expressed as

$$X(t, \omega) = \sum_{l=1}^{L} X_l(t, \omega), \tag{8.8}$$

where it is assumed that there are L rays. For different rays between the source and receiver, the ray tubes in the channel generally have little overlap. Thus, unless the scale of the environmental fluctuations is as large as the separation between rays, the micro-multipath-induced signal fluctuations in different ray tubes will show little correlation. This behavior is discussed more fully in Section 8.1.4.3.

The amplitude and spatial scale of the stochastic component of the environmental fluctuations determine the nature of the fluctuations in the micro-multipath structure of the channel. When these environmental fluctuations have a very small amplitude or the scale of the environmental fluctuations is greater than or equal to the radius of a ray tube, the signal will follow a single perturbed path within each ray tube. The channel in this case is said to be *unsaturated*. For slightly stronger fluctuations and with the same scale of fluctuations, the signal will simultaneously propagate along several perturbed paths within each tube and the perturbations in the paths will be coherent. A channel showing these characteristics is said to be *partially saturated*. If the strength of the fluctuations increases beyond this level or if the spatial scale of the environmental fluctuations becomes smaller than the radius of a ray tube while the strength of the fluctuations remains modest, the channel will be *fully saturated*. In this case, the signal will follow many perturbed paths within the ray tube, and the path perturbations will be independent.

The likelihood of encountering a fully saturated channel will increase if either the range from source to receiver is increased or the frequency of the signal is increased. Results in [25] indicate fully saturated channel conditions at a frequency of

50 kHz and range of 1 km. Reference [38] indicates the onset of full channel saturation at a range of 60 km for a frequency of 1 kHz. Analysis in [9, 10] indicates this onset at a range of around 5 km for a frequency of 20 kHz. Reference [40] reports experimental results indicating either an unsaturated or partially saturated channel at ranges of 2 to 5 km and frequency of 10 kHz. While these results provide rough guides as to what channel conditions yield saturation, the actual degree of saturation will be highly dependent on the dominant local sources of micro-multipath fluctuations in the region of propagation.

The theoretical analysis in [9, 10] does not consider the fluctuations caused by surface scattering. References [11, 12, 13, 14] as well as Chapter 9 of [2] contain explicit treatments of surface scattering effects. Experimental evidence [15] also indicates that bottom scattering can have a significant effect on the micro-multipath fluctuations in the shallow-water acoustic communications channel.

8.1.4.2 Wideband Channel Characterization

The monochromatic signal results from the preceding section can be extended to yield a wideband characterization of the channel between source and receiver [16]. The particular characterization we use is the *input delay-spread function* [17] denoted by $g(t, \tau)$ and discussed in Chapters 1 and 3. The channel input/output relationship using the input delay-spread function is

$$x(t) = \int_{-\infty}^{\infty} g(t, \tau)s(t - \tau)\, d\tau. \tag{8.9}$$

Here, $s(t)$ is the channel input and $x(t)$ is the channel output. We can see that if the input delay-spread function is independent of the time t, $g(t, \tau)$ reduces to the time-invariant impulse response. Denote the Fourier transform of $s(t)$ by $S(\omega)$ and define the *time-variant transfer function*, $G(t, \omega)$, using the Fourier transform relation

$$G(t, \omega) = \int_{-\infty}^{\infty} g(t, \tau)e^{j\omega\tau}\, d\tau. \tag{8.10}$$

It is then straightforward to show that

$$x(t) = \frac{1}{2\pi}\int_{-\infty}^{\infty} G(t, \omega)S(\omega)e^{j\omega t}\, d\omega. \tag{8.11}$$

With the Fourier transform of the transmitted signal denoted by $S(\omega)$, we can exploit the linearity of the channel to express the portion of the received signal that propagated through the lth ray tube as

$$x_l(t) = \frac{1}{2\pi}\int_{-\infty}^{\infty} S(\omega)X_l(t, \omega)\, d\omega. \tag{8.12}$$

Substituting (8.7) into (8.12) and defining

$$G_l(t, \omega) = \Psi_l(t, \omega)H_l(t, \omega) \tag{8.13}$$

yields

$$x_l(t) = \frac{1}{2\pi}\int_{-\infty}^{\infty} G_l(t, \omega)S(\omega)e^{j\omega t}\,\mathrm{d}\omega. \tag{8.14}$$

Comparing (8.11) and (8.14), we see that $G_l(t, \omega)$ is the time-variant transfer function of the lth ray tube.

To calculate the input delay-spread function of the lth ray tube, $g_l(t, \tau)$, we begin with

$$g_l(t, \tau) = \frac{1}{2\pi}\int_{-\infty}^{\infty} G_l(t, \omega)e^{j\omega\tau}\,\mathrm{d}\omega = \frac{1}{2\pi}\int_{-\infty}^{\infty} \Psi_l(t, \omega)H_l(t, \omega)e^{j\omega\tau}\,\mathrm{d}\omega. \tag{8.15}$$

Denote the *micro-multipath input delay-spread function* of the lth ray tube as $\psi_l(t, \lambda)$. Then,

$$\Psi_l(t, \omega) = \int_{-\infty}^{\infty} \psi_l(t, \lambda)e^{-j\omega\lambda}\,\mathrm{d}\lambda. \tag{8.16}$$

Substituting (8.16) into (8.15) and rearranging yields

$$g_l(t, \tau) = \int_{-\infty}^{\infty} \psi_l(t, \lambda)\left[\frac{1}{2\pi}\int_{-\infty}^{\infty} H_l(t, \omega)e^{j\omega(\tau-\lambda)}\,\mathrm{d}\omega\right]\mathrm{d}\lambda. \tag{8.17}$$

Note that the term in the brackets is the *macro-multipath input delay-spread function* of the lth ray, which we denote as $h_l(t, \tau - \lambda)$. We can then rewrite (8.17) as

$$g_l(t, \tau) = \int_{-\infty}^{\infty} \psi_l(t, \lambda)h_l(t, \tau - \lambda)\,\mathrm{d}\lambda. \tag{8.18}$$

The input delay-spread function of the lth ray tube is therefore equal to the convolution in the delay variable of the macro- and micro-multipath input delay-spread functions for the lth ray and ray tube, respectively.

Combining the input delay-spread functions for all ray tubes, the channel input delay-spread function is given by

$$g(t, \tau) = \sum_{l=1}^{L} g_l(t, \tau). \tag{8.19}$$

Figure 8.6 shows a snapshot in time of the input delay-spread functions that could correspond to the propagation paths shown in Figure 8.1. The solid black impulses represent the macro-multipath input delay-spread function for each of the rays, and the gray shaded regions represent the scaled and translated micro-multipath input delay-spread functions for each of the ray tubes. For each ray tube,

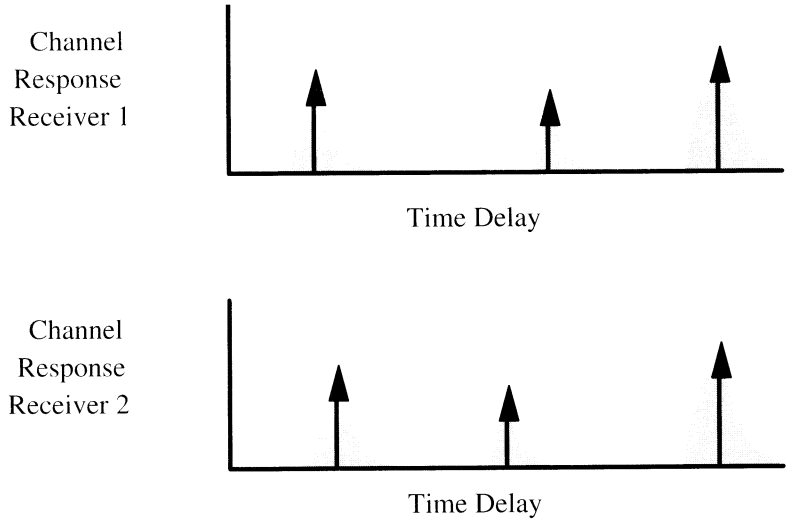

Figure 8.6 Snapshots of acoustic channel input delay-spread functions.

the total input delay-spread function is the convolution of the micro and macro-multipath functions. Note that the slowly varying macro-multipath structure influences primarily the delay and amplitude of the cluster of arrivals for each ray tube. Thus, the relative delays and amplitudes of the clusters of arrivals at one or more sensors will change on a time scale commensurate with that of the macro-multipath structure. The rapidly varying micro-multipath structure for each ray tube influences the detailed shape of the arrival for that ray tube and induces a temporal spreading of the arrivals for each tube. Thus, the particular structure of the arrivals within each cluster will change on a time-scale commensurate with the micro-multipath structure. Note that the temporal spreading function is different for each of the tubes.

Figure 8.7 shows a snapshot of the amplitude of the estimate of the complex baseband input delay-spread function for a channel in shallow water. For this example, the water depth was approximately 20 m, the distance from transmitter to receiver was approximately 200 m, and the signal covered a frequency range of 11.5 to 17.5 kHz.

Figure 8.8 shows the temporal evolution of the amplitude of the same estimated input delay-spread function over a 1.75-s interval. The estimates were made with a deterministic least squares algorithm with an averaging window of 0.02 s. The horizontal axis represents delay, the vertical axis represents absolute time, and the amplitude is represented in the gray scale. Here, there are two major clusters of arrivals. The first shows small temporal fluctuations while the second path fades in and out over intervals of 0.4 s.

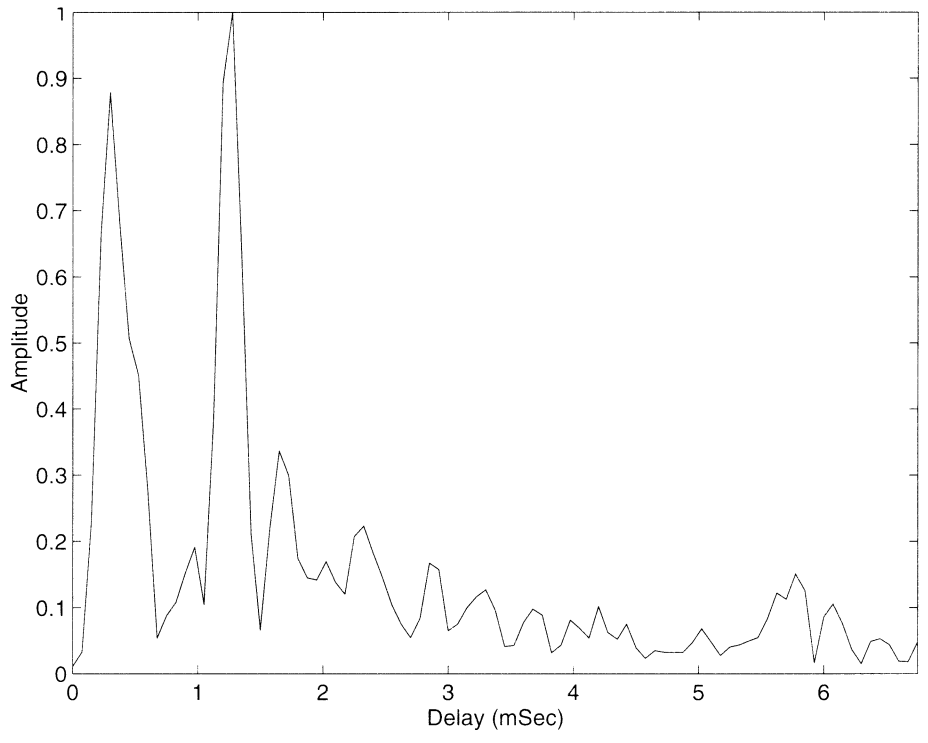

Figure 8.7 Snapshot of short range input delay-spread function.

Finally, Figure 8.9 shows the temporal evolution of the phase of the same estimated input delay-spread function.

Notice that the taps corresponding to the first significant cluster of arrivals as identified in Figure 8.8 show a slow but continuous phase drift. However, during the intervals when the taps corresponding to the second cluster of arrivals have significant amplitude, those taps show no such phase drift. The phase drift in the taps for the first cluster is the result of a Doppler shift along the corresponding ray tube and is discussed in Section 8.1.5. While the delay spread for this very short-range channel is only 6 ms, spreads exceeding 80 ms are common in longer-range channels (e.g., see Figure 8.10).

8.1.4.3 Spatial/Temporal Channel Statistics

The micro- and macro-multipath decomposition of the channel allows us to predict the spatial and temporal channel statistics as a function of the level of saturation of the channel. We can represent the input delay-spread function for a channel by clusters of taps in a tapped delay line, each tap having a time-varying and complex-valued weight applied to its output. Each cluster corresponds to the input

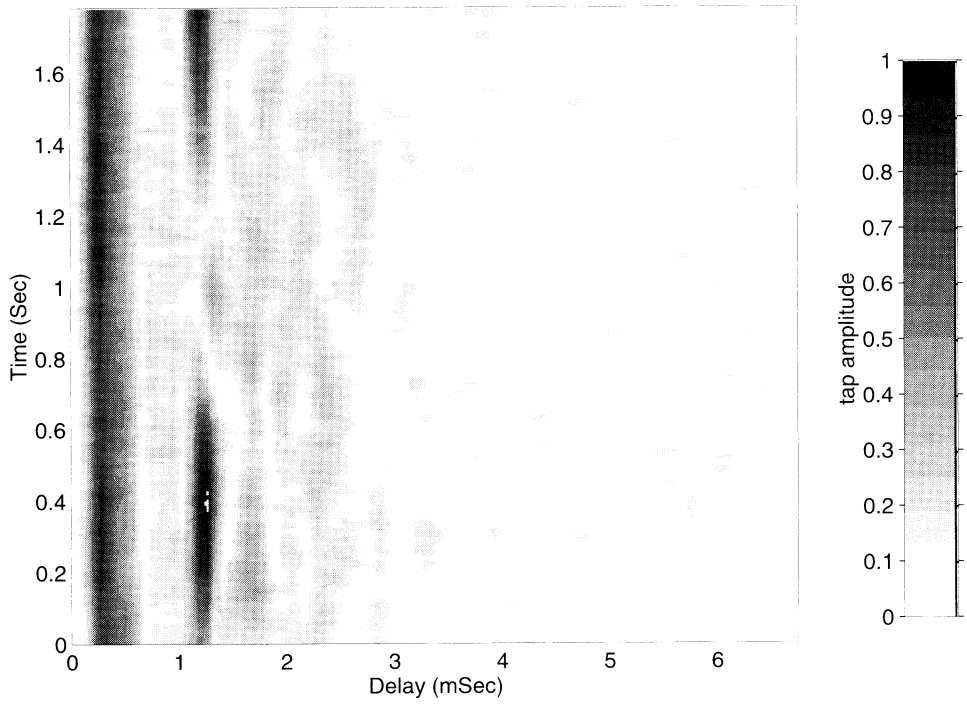

Figure 8.8 Evolution of input delay-spread function (amplitude).

delay-spread function for a particular ray tube. When the channel is either unsaturated or partially saturated, the fluctuations of the tap weights within a cluster will be coherent. However, when the channel is fully saturated, the incoherent fluctuations on each micropath within the ray tube will induce independent fluctuations in the tap weights within a cluster [25]. Whenever the spatial scale of environmental fluctuations is smaller than the separation between ray tubes, the fluctuations of the tap weights in different clusters will be independent of one another.

When examining the coherence among tap weights corresponding to the channels from a transmitter to two spatially separated receivers, we must first establish a pairing of the clusters of arrivals in each of the channels. Assume that we start with the two receivers located at the same point and establish a pairing between the individual clusters of arrivals at each receiver. Then, as we move one of the receivers and adjust the ray tubes to follow that receiver, we maintain the same pairings between the clusters of arrivals at that receiver and the clusters of arrivals at the stationary receiver. As long as the adjusted ray tube in a pair can be treated as a continuous perturbation of the original ray tube, we may continue to treat the two clusters of arrivals corresponding to the two ray tubes as belonging

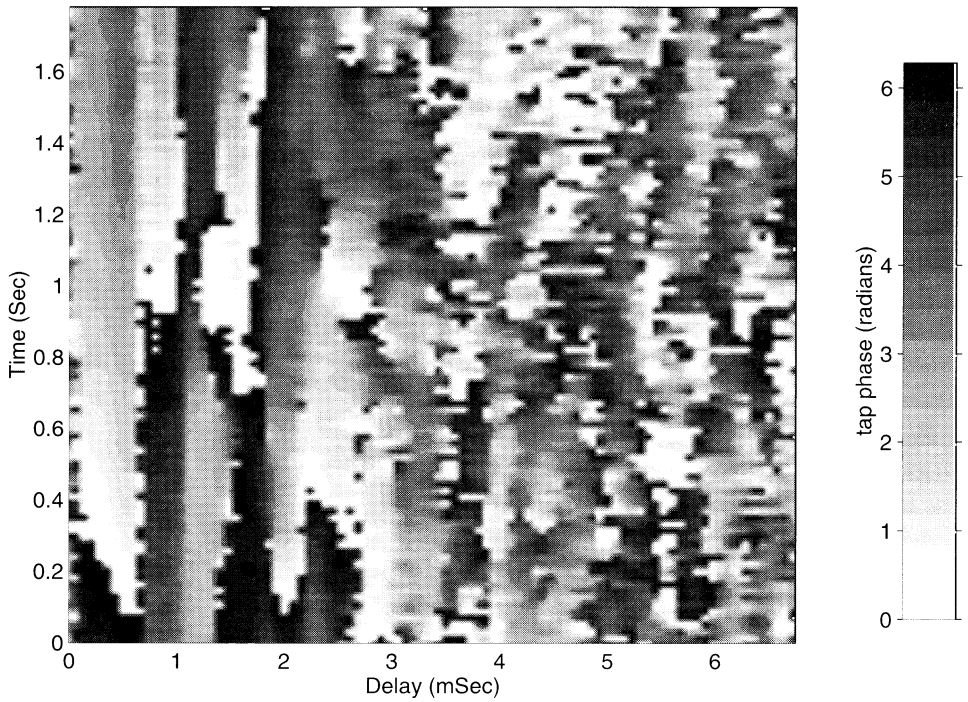

Figure 8.9 Evolution of input delay-spread function (phase).

to the same basic ray. When the channel is either unsaturated or partially saturated, there will exist some coherence between the tap weight fluctuations for the clusters of arrivals at each receiver belonging to the same basic ray. This coherence will decrease as the spatial separation of the receivers increases. At some point, when the separation between the paired ray tubes exceeds the spatial scale of the environmental fluctuations, this coherence will be lost. When the channel is fully saturated, coherence between the corresponding taps of paired clusters will be lost whenever the receivers are separated.

For the case of unsaturated or partially saturated channels, it is interesting to compare the interpath coherence at a single sensor (i.e., the coherence between taps in different clusters at one receiver) with the intersensor coherence for a single path (i.e., the coherence between taps in paired clusters at different receivers). Our analysis above tells us that for channels that are not fully saturated, the intersensor coherence for a single path will be greater than the interpath coherence at a single sensor. This coherence structure can be exploited in the development of multichannel demodulation algorithms, as discussed in Section 8.4.4.

Correlation analysis of the estimates of the input delay-spread function, using the same experimental data used to generate Figures 8.7 through 8.9, gives

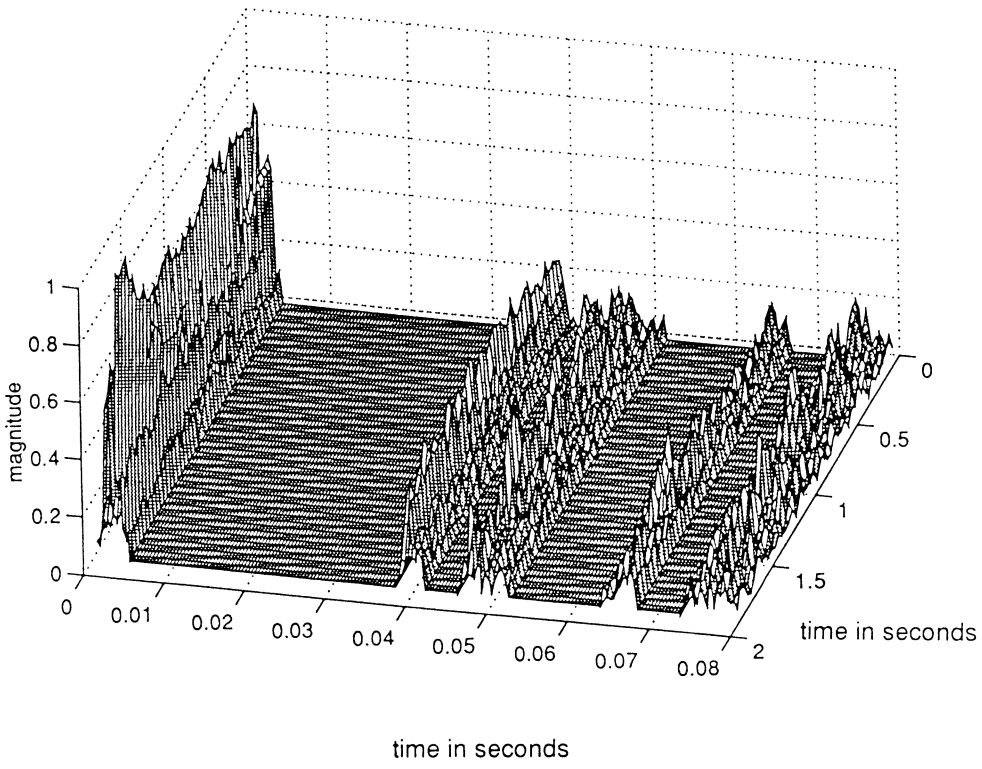

Figure 8.10 Sparse channel estimate history.

us examples of this coherence structure. The transmitted signal was received at 4 sensors. The sensors were located on a vertical line with an intersensor spacing of 1 m (approximately 10 wavelengths at the center frequency). For each sensor, the taps corresponding to the largest clusters of arrivals were identified. In each case, there were two significant clusters of arrivals. Let the estimate of the mth significant tap of the complex baseband, discrete-time input delay-spread function for the kth sensor at time n be denoted by $g_{k,m}[n]$. Assuming that there are M significant taps, we let

$$\mathbf{g}_k[n] = \begin{bmatrix} g_{k,1}[n] \\ \vdots \\ g_{k,M}[n] \end{bmatrix}.$$

The time-averaged auto- and cross-correlation coefficient matrices for $\mathbf{g}_1[n]$ through $\mathbf{g}_4[n]$ are shown in Figure 8.11. The top row contains the auto-correlation coefficient matrices. The second row shows the cross-correlation matrices between $\mathbf{g}_1[n]$ and $\mathbf{g}_2[n]$ through $\mathbf{g}_4[n]$. The third row shows the cross-correlation matrices

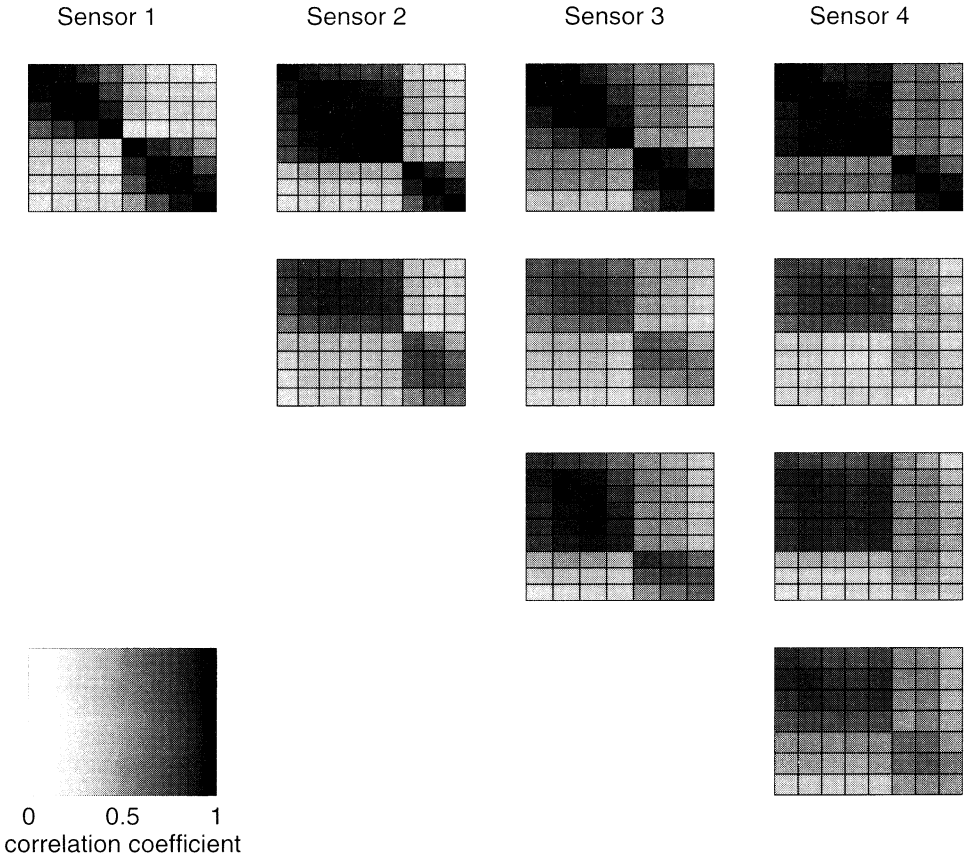

Figure 8.11 Channel tap correlation coefficient matrices.

between $\mathbf{g}_2[n]$ and $\mathbf{g}_3[n]$ and between $\mathbf{g}_2[n]$ and $\mathbf{g}_3[n]$. Finally, the fourth row shows the cross-correlation matrix between between $\mathbf{g}_3[n]$ and $\mathbf{g}_4[n]$. In all cases, the coherent averaging window was 1 s.

The block diagonal correlation structure of the matrices in the first row clearly shows the strong correlation between the taps belonging to the same ray tube and the much weaker correlation between the taps belonging to different ray tubes. Notice that for some of the matrices, the off-diagonal elements for one of the clusters of arrivals are slightly smaller than those for the other cluster, indicating a higher level of saturation for the ray tube corresponding to the cluster with the smaller off-diagonal elements. As predicted by our analysis above, the intersensor correlation for the taps in the first cluster of arrivals at each sensor is much stronger than the interpath correlation at each sensor. However, note that the taps in the second cluster of arrivals at the fourth sensor have a relatively weak correlation with the corresponding taps at the other sensors, indicating either a higher level of

saturation on the corresponding ray tubes or a greater spatial separation between these ray tubes. The significant spatial coherence between arrivals at locations separated by 10, 20, and 30 wavelengths implies strong possibilities for coherent spatial filtering with arrays of receivers. In addition, it implies that significant separations between receivers are necessary for spatial diversity techniques which rely on independent channel fading to be effective.

Strong spatial coherence over an even larger effective aperture has been reported from another experiment [18]. In this experiment, the range from source to receivers was 660 m, the water depth was 17 m, the frequency of transmission was 86 kHz, and the two receivers were vertically separated by 0.992 m (57.7 wavelengths). Even with this large receiver separation, significant coherence between the signals received at the two sensors was observed.

8.1.4.4 The Vertical Multipath Channel

The preceding discussion of the characteristics of the multipath channel is most applicable to the horizontal channel (i.e., the case where the primary spatial separation between the transmitter and receiver is in the horizontal dimension). However, in some cases, the transmitter and receiver lie on a nearly vertical line and their spatial separation is primarily vertical. The multipath characteristics of the resulting vertical channel can deviate significantly from those described above.

The difference in characteristics of the horizontal and vertical channels is primarily due to the different scales of environmental fluctuations in the horizontal and vertical dimensions. In general, the horizontal gradient of these fluctuations is much smaller than their vertical gradient. Thus, ray paths connecting a source and receiver that lie in a vertical line will have little refraction, and the cluster of arrivals corresponding to a ray tube will show little spreading. The multipath that does exist will be due to successive reflections of the sound off the sea surface and sea floor. The resulting multipath structure will show narrow clusters of arrivals separated by the round-trip propagation time from the receiver to either the sea surface or sea floor. There will be almost no arrival energy in the spaces between the clusters. The input delay-spread function of the channel will thus have a sparse structure in the delay parameter. Algorithms exploiting this sparse structure are discussed in Section 8.4.2.

8.1.5 Doppler Effects

Until now, we have not paid special attention to channel fluctuations caused by relative motion of the transmitter, receiver, or significant scattering surfaces in the environment. As discussed in earlier chapters, when any of these objects moves in

a manner that causes an increase (or decrease) in the length of a propagation path between the source and receiver, it induces a corresponding expansion (or compression) of the time axis for the received signal. That is, if the speed of sound propagation is c m/s, the length of a single propagation path is increasing at a rate of v m/s, and the narrowband signal $\mathrm{Re}[s(t)e^{j\omega_0 t}]$ is transmitted, then the noiseless, undistorted received signal will be[2]

$$r(t) = \mathrm{Re}\left[s(t(1 - v/c) - \tau_o)e^{j\omega_0 t(1-\frac{v}{c}) - j\omega_0\tau_0}\right],$$

where τ_o is a fixed delay. If the bandwidth of $s(t)$ is small with respect to its center frequency this scaling of the time axis is modeled as a frequency shift of the signal. That is, the received signal is given by

$$r(t) = \mathrm{Re}\left[s(t - \tau_o)e^{j\omega_0 t(1-\frac{v}{c}) - j\omega_0\tau_0}\right].$$

The mean of the frequency shift of the signal over some window of time is referred to as the *Doppler shift* of the signal. Removing this mean, the remaining frequency fluctuations in the signal are referred to as the *Doppler spread* of the signal. A significant source of Doppler spread is the scattering of the sound by the time-varying sea surface. See [23] for a discussion of this type of Doppler spread.

If a receiver does not compensate for the Doppler shift in the received signal, there remains an apparent phase rotation in the tap weights of the channel input delay-spread function at a rate of $e^{-j\omega_0 \frac{v}{c} t}$. Assuming a center frequency of $\omega_0/2\pi = 15$ kHz, the Doppler shift associated with a velocity of 1 m/s is approximately 10 Hz. Such a phase rotation of the taps of a channel can cause severe tracking problems with many adaptive algorithms. However, an important property of this type of time variation is that it is highly correlated from tap to tap. The recognition and exploitation of this fact in [44] led to a suitable equalizer structure for phase-coherent communications and is discussed in Sections 8.3 and 8.4.1.

In some situations, the different clusters of taps associated with different ray tubes can experience different Doppler shifts. A simple example of this is the situation where two ray tubes lead from the transmitter to the receiver. The first tube goes upward from the transmitter, bounces off the sea surface, and is reflected down to the receiver. The other tube goes down from the transmitter, bounces off the sea floor, and is reflected up to the receiver. Then, if the transmitter moves in an upward direction, the channel taps associated with the first tube will experience a negative Doppler shift while the taps associated with the second tube will experience a positive Doppler shift. Recent research has indicated that the techniques

[2]As in previous chapters, $\mathrm{Re}[\cdot]$ and $\mathrm{Im}[\cdot]$ denote the real and imaginary parts, respectively, of their complex arguments.

developed in [44] and described in Section 8.4.1 are often incapable of providing reliable communications when such multiple Doppler shifts are present [19].

8.1.6 Channel Latency and Coherence Times

A final distinguishing characteristic of the underwater acoustic channel is the relationship between the channel latency (i.e., the time it takes for a signal to propagate through the channel) and the coherence time of the channel fluctuations. Data presented and referenced herein indicate that the characteristics of a channel can change significantly in one-half of a second or less. However, for a channel with a range of just 1 km, the one-way propagation time from transmitter to receiver is greater than two-thirds of a second. Therefore, in many situations, the channel can change significantly in the time it takes for the signal to propagate from the transmitter to the receiver. Such a situation makes it difficult to implement modulation or coding algorithms that require accurate knowledge of the particular realization of the channel through which communication is being attempted. Platform motion can also have a significant effect on multiple-access techniques that require precise timing of signal receptions. Motion of just a single meter can shift the arrival time of a signal by two-thirds of a millisecond. This shift can span many channel symbols in a high-rate system and can occur in much less time than it takes a signal to propagate through all but very short-range channels. Thus, the synchronization of the user's transmissions to achieve reception without multiple-access interference or the use of significant guard bands will be difficult in many channels.

8.2 Platform Constraints in Underwater Acoustic Communications

Many applications of underwater acoustic communications involve communication with or between autonomous underwater vehicles or remotely deployed instrumentation. In both situations, the communications system faces significant constraints on the permissible size of the communications equipment and on the power available to this equipment.

The size constraint can limit the choice of the operating frequency of the system. In general, the power efficiency of an acoustic transducer is proportional to the ratio of its size to the acoustic wavelength. So, in order to obtain an efficient transducer with which to transmit the sound, a high frequency must often be used. However, the high-frequency sound will experience greater attenuation in the water than would lower-frequency sound. Thus, the frequency must be chosen to obtain a balance between transducer efficiency and signal absorption.

The constraint on available power most obviously limits the signal energy that can be radiated. However, this constraint also places limits on the complexity of the modulation and demodulation algorithms that can be used in a system. In general, the power consumed by a processor is proportional to the computational capability provided by that processor. Thus, the power constraint also constrains the computational capability available to implement modulation and demodulation algorithms. Combining the rapidly changing multipath channels whose delay spreads approach a hundred symbols with significant power limitations on oceanographic instrumentation or autonomous underwater vehicles, the computational complexity of demodulation algorithms can quickly exceed the available computational capability. For this reason, the development of computationally efficient algorithms is an important and active area of research. Some past and current work in this area is discussed in Sections 8.4.2 and 8.4.4.

8.3 A Brief History of Underwater Acoustic Communications

There has been considerable progress in improving communications over the channels discussed in the preceding sections. Here we identify those communication techniques that have advanced the field. This section is not intended to be an exhaustive historical review, and the reader is directed to [21] for a review of underwater acoustic communications prior to 1967, to [22] and the references therein for a review of acoustic telemetry prior to 1983, to [23] for a review of recent advances in phase-coherent underwater acoustic communications, and to the articles in [24] for reviews of modulation techniques, equalization and coded modulation as applied to the UAC.

Underwater acoustic communication systems can be classified according to how the transmitter and receiver combat the effects of multipath fading. Important to this classification is the concept of *diversity*, which, as discussed in Chapter 1, is the transmission of the communication message through independently faded channels [31]. *Explicit diversity* is characterized by intentional transmissions through distinct subchannels in time, frequency, geometric space, or waveform space. Due to the independence of the subchannel fading processes, the channel error probability is exponentially decreasing in the number of retransmissions, or diversity order. Coding across these subchannels (other than repetition coding) is known to make efficient use of the channel bandwidth [31]. *Implicit* diversity can be achieved by spectrally spreading the message signal over a single transmission band having a width W much larger than the coherence bandwidth of the channel. This wideband signal can be used at the receiver to resolve and identify the individual multipath arrivals spaced in delay by more than $1/W$ [32]. If these complex amplitudes can be

accurately estimated and tracked, a receiver can use implicit diversity to achieve an error-rate improvement identical to that of explicit diversity [33]. Using the concept of diversity, underwater acoustic communication systems can be grouped into three classes, as to whether the links use (1) no diversity techniques, (2) only explicit diversity reception, or (3) at least implicit diversity processing.

The first class of underwater acoustic communication systems includes those that did not employ diversity techniques. This class includes most of the early analog communication systems, which used careful hydrophone placement to compensate for multiple path propagation via distinct angles of arrival. The development of reliable underwater acoustical communications began after World War II with the Gertrude, an analog, amplitude-modulation system that permitted communication to submarines [25]. Single-sideband derivatives of the Gertrude are still used in modern diver communication systems [26] and perform well for vertical or ultrashort-range horizontal links with negligible multipath propagation.

Several digital underwater acoustic communication systems also belong to this first class. The development of digital UAC links were reported as early as 1960 [27, 28]. These systems dealt with multipath by acoustic baffling and by using very low rate channel codes [29]. A typical digital communication system of this type, described in [30], permitted 4800 bits per second (BPS). Early implementations of multiuser detectors for UACs did not employ diversity methods and minimized multipath-induced distortion by transmitting vertically through the water column [36]. Digital communication links through horizontal, shallow-water channels have also been designed without diversity techniques [39]. In this case, multipath propagation was avoided through the use of many transmit transducers.

The second class of underwater communication systems use explicit diversity reception. Most of these systems employed digital modulation. Perhaps the most carefully documented communication link of this class is the digital acoustic telemetry system (DATS) [34]. The DATS was designed for transmission of digital data in an environment that exhibited frequency-selective multipath fading and extreme phase instability. The DATS transmitted coded data using on-off, multiple-frequency shift keying modulation in the 45–55 kHz frequency band, provided a coarse word synchronization reference with a gated 30 kHz header tone, and a provided continuous 60 kHz pilot tone for Doppler tracking. In one implementation of DATS, a 400 BPS digital data stream was transmitted at a baud (symbol) rate of 100 Hz by encoding 4 bits per baud with an (8,4)-Hamming code. The Hamming codeword elements selected from eight tones spanning 2 kHz at each baud period. A slow frequency-hopping scheme translated the set of eight tones for each baud period to minimize intersymbol interference. The receiver coherently estimated the Doppler shift with a phase-locked loop (PLL) whose output was used to adapt the downconversion carrier, nominally at 50 kHz. The DATS detector tracked the hopping pattern to determine the frequency span for the current word and implemented

an inverse FFT to extract the squared magnitudes of the received gated tones. Noncoherent, soft-decision detection was used to estimate the 8-bit codeword.

Since the coherence bandwidth of the UAC in [34] was 2 kHz, the above system did not utilize frequency diversity per se. However, trivial changes in the implementation would permit eightfold diversity reception. Variants of this communication system are still under investigation [35]. Several commercially produced acoustic modems follow the DATS format and permit reliable transmission through highly reverberant multipath channels at modest complexity [37]. This communication link is quite insensitive to Doppler shifts as well. In the configuration described above, the DATS system can tolerate about 600 Hz of Doppler shift if the PLL is successfully tracking the pilot tone, and about 25–50 Hz of Doppler shift when the pilot PLL loses lock on the received tone. Since 0.5 m/s corresponds to 17 Hz of Doppler shift for an underwater acoustical tone at 50 kHz, this Doppler tolerance translates to a relative platform drift between 1 m/s and 8 m/s. Other configurations of the DATS have been reported for deep water channels [43].

The third class of underwater acoustic communication systems includes those modems that utilize implicit diversity reception. Specific examples of implicit diversity reception include RAKE filtering, fractionally spaced decision-feedback equalization, wideband array processing, and echo cancellation. Explicit diversity reception can be used in these systems as well. Digital underwater acoustic links in this class have demonstrated the greatest spectral efficiency to date (measured in BPS per Hertz of transmission bandwidth) of all systems operating with the same number of sensor elements, input signal-to-noise ratio (SNR) and bit error rate [23]. Communication links that employ implicit diversity processing have shown the greatest promise to provide reliable, high-speed, and power-efficient links. As of this writing, research is most active for these types of communication systems, and digital signal processing techniques for implicit diversity systems are the focus of the remainder of this chapter.

Perhaps the earliest reference to single-sensor implicit diversity for UACs is [41]. In that work, coherent echo cancellation compensated for intersymbol interference in a phase-shift keying (PSK) communication system. References to adaptive equalization as a means to provide high-speed underwater acoustic communications appeared in the literature in the early 1990s [42]. Much work has been done on the development of demodulation algorithms for multichannel receivers, and it remains an area of active research [16, 39, 45, 47, 86, 87, 88, 89, 90].

An impetus for current signal processing research in UACs is provided by the results in [44] for single-sensor reception and [45] for multisensor reception. These works demonstrated the feasibility of high-rate phase-coherent digital communications through highly reverberant shallow-water channels, by means of adaptive channel equalization. With regard to current research in this field, the most important contribution of [44] was a decomposition of the time-varying input

delay-spread function of shallow-water channels into two tandem subsystems: a complex baseband input delay-spread function whose coherence time spanned hundreds of milliseconds, and a unit-gain complex amplifier whose instantaneous phase is approximately affine over tens of milliseconds. This second subsystem accounts for the Doppler shift introduced by relative platform motion, as was discussed in Section 8.1.5. Prior to this work, it was thought that shallow-water channel taps exhibited mutually uncorrelated temporal trajectories, both in magnitude and phase. Adaptive channel identification under this hypothesis would usually not produce convergence within the coherence time of the overall channel. In hindsight, the (common) phase variation of all taps yielded a rapidly time-varying channel over the averaging window for the estimator. The work in [44] presented the first demonstrable evidence that the phase trajectories for significant input delay-spread function taps were strongly correlated and that the common phase rotation of these taps could be tracked by a single, second-order, digital PLL. Employing a common phase correction, an adaptive, fractionally spaced, decision-feedback equalizer (DFE) was shown to converge and compensate for the channel distortion. Convergence of equalizer taps is not possible in some shallow-water channels without this phase compensation. This result is quite different from equalization for twisted-pair links, whose (few) equalizer taps may converge in the absence of common phase tracking, even for similar frequency offsets. An analysis of the effects of residual phase errors on adaptive equalization is presented in [46].

8.4 Signal Processing in Digital Underwater Communications

In the remainder of this chapter, we describe some of the ways that advanced signal processing can enhance the performance of underwater communication systems.

8.4.1 Detection of Linear Digital Modulation

We begin by reviewing the detection strategy presented in [44] for coherent detection of single-sensor reception of linear digital modulation. Multisensor reception is reviewed in another section. Both the channel model and the adaptive filtering metric are described in the deterministic, weighted least squares framework. Provided a scalar $\lambda \in (0, 1)$, there is a temporal window ending at time t_0 and having an approximate duration of $T/(1-\lambda)$ seconds, over which the baseband complex channel output is modeled as

$$\begin{aligned} r(t) &= \sum_n d_n g(t, t - nT) + n(t) \\ &\approx \sum_n d_n h(t - nT) e^{j\varphi(t)} + n(t), \quad t - t_0 \in [-T/(1-\lambda), 0). \end{aligned}$$

Here, $g(t, \tau)$ denotes the input delay-spread function as discussed in Section 8.1.4.2, $\{d_n\}_{n=-\infty}^{n_0-1}$ represents a known or accurately detected complex symbol sequence, $\lfloor n_0 - t_0/T \rfloor = 0$, T denotes the channel symbol (or baud) period, $\varphi(t)$ is an unknown affine function described in Section 8.1.5, $h(\tau)$ is an unknown, deterministic, time-invariant impulse response, and $n(t)$ is baseband, complex, stationary Gaussian noise with a flat power spectral density over the transmission bandwidth. It is assumed that the "forgetting factor" λ was chosen to maximize the temporal window width for which $g(t, \tau) \approx h(\tau)e^{j\varphi(t)}$. It is also assumed that coarse synchronization has provided an approximate temporal reference for the impulse response and that Doppler compression is expressed as a phase rotation. Coarse synchronization may be achieved by preceding a data packet by a brief signal whose energy spectral density is broad.

An adaptive, fractionally spaced, DFE was proposed in [44] as a receiver structure and is shown in Figure 8.12.

The feedforward filter samples the observation at rate $1/T_s$, an integer multiple of the symbol rate $1/T$, and produces outputs at times nT. After phase correction, the output at time n_0T is p_{n_0}, where[3]

$$\begin{aligned} p_n &= \mathbf{a}^H \mathbf{r}(n, \tau) e^{-j(\omega_d n + \theta)}, \\ \mathbf{r}(n, \tau) &= [r(nT + N_1 T_s + \tau) \ \cdots \ r(nT - N_2 T_s + \tau)]^T, \end{aligned} \tag{8.20}$$

where $\mathbf{a}$, ω_d, and θ and τ are filter coefficients. The fractionally spaced front end is especially adept at correcting for an error between τ_n and the true timing phase [48]. The filter's temporal span $T_s(N_1 + N_2 + 1)$ should be chosen to allow

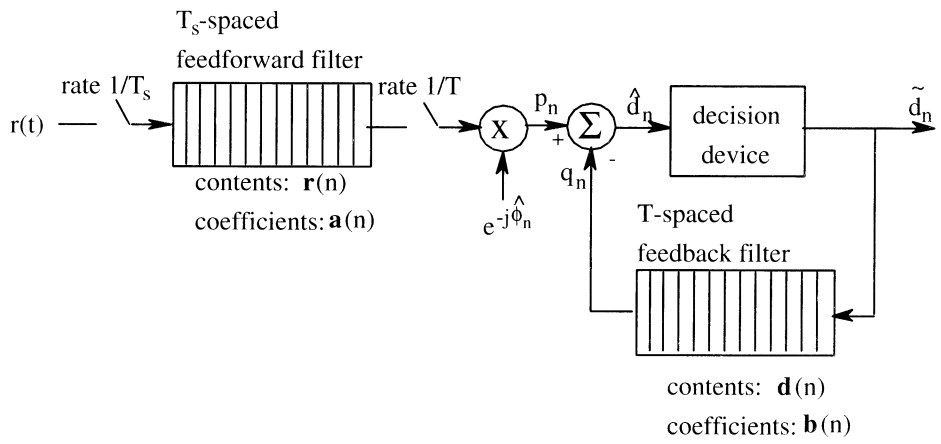

Figure 8.12 Adaptive, fractionally spaced, decision-feedback equalizer.

[3]The superscript ^{H} denotes the conjugate-transpose operator. The superscript ^{T} denotes the transpose operator.

for nonminimum phase responses, such as the one shown in Figure 8.9, and residual timing jitter due to Doppler dilation/compression.

The feedback filter in Figure 8.12 linearly combines M previous symbol decisions to suppress residual causal intersymbol interference and forms q_{n_0} at time n_0T, where

$$\begin{aligned} q_n &= \mathbf{b}^H \mathbf{d}(n) \\ \mathbf{d}(n) &= [\tilde{d}_{n-1} \quad \cdots \quad \tilde{d}_{n-M}]^T. \end{aligned} \tag{8.21}$$

The complex predecision variables $\hat{d}_n = p_n - q_n$ are quantized to form final decisions $\tilde{d}_n$.

The adaptation rules presented in [44] yield extremal solutions for the deterministic weighted squares metric

$$\mathcal{J}_n(\mathbf{a}, \mathbf{b}, \tau, \omega_d, \theta) = \sum_{k=0}^{n} \lambda^{n-k} \left| \tilde{d}_k - \mathbf{a}^H \mathbf{r}(k, \tau) e^{-j(\omega_d k + \theta)} + \mathbf{b}^H \mathbf{d}(n) \right|^2. \tag{8.22}$$

Gradients of $\mathcal{J}_n$ with respect to the receiver parameters can be obtained directly from the observations and take the form[4]

$$\begin{aligned} \frac{1}{2}\nabla_{\mathbf{a}}\mathcal{J}_n &= \left(\sum_{k=0}^{n} \lambda^{n-k} \mathbf{v}(k)\mathbf{v}^H(k) \right) \mathbf{a} - \left(\sum_{k=0}^{n} \lambda^{n-k} \mathbf{v}(k)\mathbf{d}^H(k) \right) \mathbf{b} - \left(\sum_{k=0}^{n} \lambda^{n-k} \mathbf{v}(k)\tilde{d}_k^* \right), \\ \frac{1}{2}\nabla_{\mathbf{b}}\mathcal{J}_n &= \left(-\sum_{k=0}^{n} \lambda^{n-k} \mathbf{d}(k)\mathbf{v}^H(k) \right) \mathbf{a} + \left(\sum_{k=0}^{n} \lambda^{n-k} \mathbf{d}(k)\mathbf{d}^H(k) \right) \mathbf{b} + \left(\sum_{k=0}^{n} \lambda^{n-k} \mathbf{d}(k)\tilde{d}_k^* \right), \\ \frac{\partial}{\partial\theta}\mathcal{J}_n &= +2 \operatorname{Im}\left[\sum_{k=0}^{n} \lambda^{n-k} p_{k,n} e_{k,n}^* \right], \\ \frac{\partial}{\partial\omega_d}\mathcal{J}_n &= +2 \operatorname{Im}\left[\sum_{k=0}^{n} \lambda^{n-k} k p_{k,n} e_{k,n}^* \right], \\ \frac{\partial}{\partial\tau}\mathcal{J}_n &\approx +2 \operatorname{Re}\left[\sum_{k=0}^{n} \lambda^{n-k} \frac{p_{k,n} - p_{k-1,n}}{T_s} e_{k,n}^* \right], \end{aligned} \tag{8.23}$$

where $p_{k,n} = \mathbf{a}^H(n)\mathbf{v}(k)$, and $e_{k,n} = p_{k,n} - \mathbf{b}^H(n)\mathbf{d}(k) - \tilde{d}_k$. In these equations, we have made the substitution $\mathbf{v}(k) = \mathbf{r}(k, \tau)e^{-j(\omega_{d,n}k + \theta_n)}$, and we have suppressed the notational dependence of $\mathbf{v}$ on the receiver's phase and synchronization parameters. We have denoted extremal values of filter parameters for cost $\mathcal{J}_n$ with the index n in the defining expressions for $p_{k,n}$ and $e_{k,n}$. A backward difference approximates the for-

[4]The gradient of $\mathcal{J}$ with respect to a complex vector $\mathbf{v} = \mathbf{x} + j\mathbf{y}$ is defined as $\nabla_{\mathbf{v}}\mathcal{J} = \nabla_{\mathbf{x}}\mathcal{J} + j\nabla_{\mathbf{y}}\mathcal{J}$. A complex vector $\mathbf{w}$ is normal to this gradient if $\operatorname{Re}(\mathbf{w}^H\nabla_{\mathbf{v}}\mathcal{J}) = 0$.

mal derivative in the last expression. The gradients for **a** and **b** are usually decoupled from the unknowns θ, ω_d, and τ by use of precomputed estimates. The extremal equations for **a** and **b** can be rewritten to reveal the recursive structure of their solutions,

$$\begin{aligned}
&\mathbf{R}(n)\begin{bmatrix}\mathbf{a}\\ \mathbf{b}\end{bmatrix} = \mathbf{y}(n),\\
&\mathbf{y}(n) = \lambda\mathbf{y}(n-1) + \tilde{d}^*(n)\begin{bmatrix}\mathbf{v}(n)\\ -\mathbf{d}(n)\end{bmatrix}, \quad \mathbf{y}(-1) = \mathbf{0},\\
&\mathbf{R}(n) = \lambda\mathbf{R}(n-1) + \begin{bmatrix}\mathbf{v}(n)\mathbf{v}^H(n) & -\mathbf{v}(n)\mathbf{d}^H(n)\\ -\mathbf{d}(n)\mathbf{v}^H(n) & \mathbf{d}(n)\mathbf{d}^H(n)\end{bmatrix}, \quad \mathbf{R}(-1) = \mathbf{0}.
\end{aligned} \tag{8.24}$$

The sequence of extremal equalizer parameters $\{\mathbf{a}(n), \mathbf{b}(n)\}$ can be found by any version of the recursive least-squares (RLS) algorithm, as this structure shows. A numerically stable implementation of an order $10N$ (per update) RLS algorithm was suggested for the shallow-water acoustic channel [44], and a development of this algorithm can be seen in [50]. Here, N is the number of real coefficients in the recursion $2(1 + N_1 + N_2 + M)$. Estimation for the synchronization and phase can proceed in a variety of ways. For modest Doppler shifts, the phase estimate can be obtained via a second-order phase-locked loop (to track the affine trajectory). The synchronization update can be achieved by an early delay-lock loop, as suggested by the gradient $\partial\mathcal{J}_n/\partial\hat{\tau}_n$. An extension of these results can be found in [45] for the multiple-sensor case and in [51] for high Doppler environments.

Adaptive linear equalization has also been applied successfully to the vertical acoustic channel, which usually exhibits longer coherence times. Since the direction of propagation is tangential to the thermal gradient, multipath due to refraction is minimal. However, transmission from mid-depth to the surface is known to produce an extremely high multipath spread due to bottom reflections, as discussed in Section 8.1.4.4 and in [52]. In at least three instances, coherent or differentially coherent phase modulation was achieved in the vertical acoustic channel by adapting a linear equalizer according to a least mean squares (LMS) algorithm for well-conditioned input data [52, 53, 54]. The extremal conditions for linear equalization may be seen by forcing $\mathbf{b} = \mathbf{0}$ and ignoring the gradients for $\mathbf{b}_n$ in (8.23). Several approaches suggest self-adaptive versions of the LMS algorithm, which varies the step sizes for each gradient in order to reduce both the convergence time and tracking error, e.g., [52]. The reader is referred to [55] for a review of self-adaptive LMS algorithms and to [56] for a review of the convergence and tracking properties of the LMS family of algorithms.

The work in [44] has suggested that RLS-based adaptive equalization is required for rapidly varying shallow-water acoustical channels. Once the channel taps are derotated by the phase compensator, as shown in Figure 8.12, then the

coherence time of the residual channel is lengthened considerably and permits accurate channel tracking. Despite several well-known reports of the superior convergence properties of RLS algorithms over LMS algorithms [31], there exists a preference for the latter in the underwater acoustic communications literature. Most authors prefer LMS because of the order $O(N)$ complexity (floating-point operations (flops) per update) of LMS to the order $O(N^2)$ complexity of the (stable) conventional RLS algorithm. These authors cite improvements in convergence time of newer members of the LMS family, as reviewed in [56] and references therein. RLS proponents counter with the $O(N)$ complexity of the numerically stable, fast transversal RLS (FTRLS) algorithm [49]. At least one work has employed an RLS-based update for the feedforward taps, for which the input data is not well conditioned, and an LMS-based update for the feedback taps, for which the input data is usually white [79]. Regardless of the vantage point of these works, two attributes are considered crucial for an adaptive receiver in shallow water: fast convergence time and low computational complexity.

In the next section, we summarize research efforts to combine these features in detection algorithms. Rather than focusing on the usual attempts to reduce complexity by minimizing computational redundancies, we concentrate on work that exploits the natural sparseness of the impulse response magnitude of the UAC, as well as cases for which the baud rate dominates the Doppler spread (reciprocal coherence time) of the channel.

8.4.2 Complexity Reduction in Adaptive Detection

Implicit diversity, which is usually attained via wideband signaling, permits the resolution of paths spaced by no less than the reciprocal of the transmission bandwidth. As the channel symbol rate has increased in underwater acoustic applications during the last decade, both the channel resolution and the channel memory have increased as well. The *memory* of the communication channel refers to the multipath delay spread, normalized by the channel symbol period. The channel memory is an important characterization in partially coherent reception of linear digital modulation because the number of parameters in an adaptive receiver is typically proportional to the worst-case channel memory. For example, a fractionally spaced DFE requires enough feedforward parameters to span the group of delay taps corresponding to the principal arrival, including uncorrected tap drift, and the symbol-spaced feedback taps should span the memory of the residual impulse response. Consider a medium-range horizontal acoustic link with a worst-case multipath spread of 40 ms and a baud rate of 2,500. The channel memory for

this link is 100 channel symbols. If the $T/2$-spaced feedforward filter spans 16 channel symbols, then the dimension of the feedback filter might be as high as 120. Doubling the channel symbol rate would double the number of receiver parameters. Since it has been demonstrated that higher baud rates improve the phase tracking properties of the adaptive receiver [23], the baud rate and channel memory will tend to increase in future deployments of phase coherent systems.

We begin by establishing a complexity benchmark for our subsequent development in this section. To this end, we shall assume single-sensor acquisition and that $O(\mu)$ complex parameters will be adapted at the baud rate of R_B symbols/s (SPS) for a channel of memory $\mu = T_m R_B$, where T_m seconds is the temporal multipath spread. Regardless of whether LMS or FTRLS is used to update the receiver parameters, the computational requirements for adaptation will be proportional to $O(T_m R_B^2)$ flops per second. Thus, the computational burden imposed on battery-powered acoustic modems operating in a channel with the above dimensions is roughly 10 times that of modems in an average telephony channel operating at the same baud rate (see [31], p. 537). In addition, the demodulation complexity for a DFE is also of order $O(T_m R_B^2)$ flops per second, excluding decoding complexity. Real-time demodulation of these signals on board an autonomous undersea vehicle (AUV) requires careful design of the hardware and algorithms for onboard modems, which are usually constrained to use less than 20 W for both hardware and acoustic power.

There are two general approaches for reducing the $O(\mu R_B)$ complexity of the adaptive receiver described earlier. One class attempts to reduce the complexity through the parameter update rate, which coincides with the channel baud rate (R_B) in the above scenario. If the channel baud rate would exceed substantially the reciprocal coherence time of the channel (often called the *Doppler spread*), then the channel taps at one update time are strongly correlated with those of the previous update time, and the channel estimator (or equalizer parameters) may be updated less frequently. We describe this class as *reduced updating* techniques. While these techniques play a vital role in reducing the computational complexity in some adaptive receivers, space does not permit a thorough review of current approaches. Instead, we focus on approaches that find special application in underwater systems. This second, broader class of algorithms attempts to reduce the number of receiver parameters relative to the scenario described earlier. Through these techniques, the parameter dimension in the complexity product is considerably less than the channel memory μ. Regardless of whether LMS- or RLS-type updates are used, we also expect the convergence time to be smaller for this reduced set of receiver coefficients if the system is not underparameterized. We refer to algorithms of this type as *reduced parameterization* techniques. In the remainder of this section, we review algorithms in this class.

8.4.2.1 Reduced Parameterization Techniques

There are three well-documented approaches to the reduction of the number of receiver parameters: *waveform shaping*, *indirect adaptive equalization*, and *memory truncation*.

Waveform shaping attempts to reduce the memory of the overall input delay-spread function through signal design at the transmitter. In effect, the transmitter introduces an additional filter tandem to the communication channel, which yields an overall input delay-spread function with less memory. While this approach has been most often employed in time-invariant communication channels, it may be employed for time-varying systems, using accurate channel information supplied by the far-end receiver. In underwater systems, this enhancement may be achieved through a reverse link with a propagation delay that is less than the coherence time of the phase-compensated channel. Waveform shaping may be performed with single transducer transmission in this environment but is considerably more effective when long transmitter arrays are used, as described in [39]. As was noted in this work, this approach works best in the shallow-water channel with stationary platforms and short-range links. Latency and coherence issues for horizontal channels was presented in Section 8.1.6. For single-transducer transmission, waveform shaping may also be achieved by designing a receiver filter to produce an output with a prescribed and controlled amount of interference. With respect to overall computational burden, the trade-off in this approach, sometimes called *partial-response equalization*, balances the complexities of the front-end filter and the residual interference suppression. This distortion can be mitigated in slowly time-varying, 2-way links by *channel precoding* at the transmitter or by subsequent equalization at the receiver. As an example of the latter approach for long memory channels, a linear equalizer followed by a maximum likelihood sequence detector has been considered. Complexity was reduced in part by the design of the linear equalizer and by a reduction of memory in the subsequent dynamic programming (Viterbi) algorithm [57]. Linear partial-response equalization followed by Viterbi-type equalization has been used in a (time-invariant) magnetic recording channel to reduce complexity.

Indirect adaptive equalization has also demonstrated an ability to reduce the computational complexity in some time-varying multipath fading channels. Rather than (directly) adapting the equalizer coefficients in a receiver, this approach first identifies the unknown channel taps (using a tapped-delay-line model) and noise statistics and then sets the equalizer to compensate for the channel model. It has been demonstrated recently that the method of indirect channel equalization is more robust to the time variation of some multipath fading channels [62]. Other work has suggested that indirect adaptive DFEs may be imple-

mented at a lower computational complexity than an equalizer with directly adapted coefficients [63]. In effect, the indirect adaptation method yields fewer degrees of freedom in these circumstances, which reduces the convergence time, tracking error, and misadjustment of an adaptive algorithm. As we discuss shortly, there may be other, *channel-specific* ways to reduce the degrees of freedom of this channel identification even further.

Memory truncation is a deliberate mismatch of the receiver structure with respect to the channel model, to provide fewer adapted parameters than with an unconstrained structure. Memory truncation has traditionally been achieved by ignoring scattered paths beyond a fixed delay and advance from the principal arrival and is usually determined with a knowledge of the performance sensitivity to the receiver mismatch. Many studies of performance sensitivity to mismatch exist and quantify tolerable levels of memory truncation. The sensitivity to channel mismatch was investigated for maximum-likelihood-type receivers in intersymbol interference (ISI) channels [58, 59] and to linear equalizers and DFEs in [60, 89] and references therein.

8.4.2.2 Sparse Channel Identification

We now address current work on channel-specific approaches to parameter reduction that are especially suited for underwater acoustic applications. Of relevance are channel identification techniques that reduce the computational complexity according to the *sparseness* of slowly time-varying linear systems. For purposes of this presentation, sparseness applies to a slowly time-varying linear system if its multipath intensity profile (MIP), maximally truncated in the delay axis without loss, shows a concentration of power in relatively few taps. Intuitively, a sparse system exhibits clean echoes spaced by large temporal gaps. These gaps may incur an increase in the computational complexity for both conventional channel tracking and demodulation of linear, digital data passed through this sparse system, relative to a system possessing a similar MIP, but without the delay gaps. A typical example of a sparse system is the medium-range shallow-water UAC, and a history of input delay-spread function magnitude estimates can be found in Figure 8.10. Tap magnitudes below a very small threshold were suppressed in this figure in order to more clearly exhibit the sparse nature of the channel. Note in the figure that while the multipath delay spread for this channel exceeds 80 ms, about 12% of the channel taps contribute significantly to the output. Channels such as the UAC are especially suited for sparse channel identification techniques.

The UAC has exhibited sparseness in a variety of wideband transmission experiments. Sparseness has been observed from a surface-deployed receiver in the vertical acoustic channel, in which echoes were observed due to reflections of the transmitted signal off the sea floor [52]. The medium-range, horizontal UAC

has also exhibited sparseness for shallow-water transmissions near Fort Lauderdale, Florida [66], New England harbor sites [64] and for deep-water transmissions in the Arctic circle [65]. A presentation of sparse UACs can be found in [67]. While an underwater channel is not always sparse, it can be approximated as sparse with enough frequency to motivate an incorporation of sparse techniques into wideband acoustic modem designs [66]. An ideal algorithm for sparse channel identification would include full-order identification as a special case and would permit low convergence times for all system orders. In this section, we shall refer to a channel identification technique as a *sparse channel identification* algorithm if it exploits the sparseness in a system to reduce the computational complexity, convergence time, or estimation error. Sparse adaptive equalization will refer to similarly tailored techniques for coherent demodulation of linear, digital modulation through sparse dispersive systems.

There is a significant amount of prior work on rapidly converging or low complexity channel identification for sparse systems. In some of these cases, prior knowledge about the channel is presumed, such as the number of significant input delay-spread function taps (the system order), their location in delay, or the system multipath spread. In short, all of these (or their approximations) may be provided without major changes of several current modem designs [66]. These modems will initiate communication by preceding a phase-modulated data packet with a packet consisting of a short carrier-modulated Barker sequence followed by a silent period. While the purpose of the Barker sequence is to remove the receive modem from standby mode, a temporal window of the observation (or its correlation magnitude with the Barker sequence) can be stored for future processing. This magnitude sequence provides an estimate of system order, approximate locations of significant taps, and delay spread.

Reference [70] proposed a method of sparse channel identification that increments the order of the channel estimator until a prescribed squared-error criterion is satisfied. At each increment, the best delay for a new input delay-spread function tap is determined, using a criterion that is independent of this tap's magnitude and phase. Once the best tap location is determined, the magnitude and phase are estimated. This approach is suited for very sparse systems, and its order-recursive approach may impose a lengthy convergence for full-order systems. However, this technique is quite effective in rapidly identifying the location of a new tap in other sparsing methods. At least three independently derived efforts in sparse adaptive equalization appeared during the same year, suggesting that the solution had strong relevance [64, 76, 77]. In [77] and in subsequent work [52], a sparse implementation of an adaptive linear equalizer was considered for suppression of intersymbol interference in a vertical acoustic channel. Direct adaptive equalization was implemented, and the coefficients of the symbol-spaced transversal filter were adjusted with the LMS-based stochastic-gradient algorithm with time-varying step

sizes. Time was partitioned into epochs lasting hundreds of symbols, over which the channel is presumed to be statistically stationary. The approach in [77] tailored its complexity for sparse systems by selecting a different subset of the transversal filter taps to adapt during each of these epochs. The two largest tap magnitudes are selected from an estimation of the transversal filter taps at the beginning of an epoch; from the relation $\frac{1}{1-z^{-D}} = 1 + z^{-D} + z^{-2D} + \cdots$, $|z| < 1$, the tap delay spacing D between these two taps estimates the multipath delay spread of a 2-tap system and, hence, the spacing of significant taps in a suitable zero-forcing equalizer (high SNR is presumed). These two taps and those at delays $2D$, $3D$,... are updated during this epoch, and the remaining taps are fixed. The work demonstrated successful, low-complexity demodulation of 4-PSK data in both 2- and 3-path channels using this approach, and comparisons between full-order filter updates and the sparse approach showed little performance degradation.

Identification of sparse systems is also an active topic of research in the controls area, where it is motivated from a model-reduction perspective [71, 72, 73, 74, 75]. A model-reduction approach was used to develop the sparse adaptive equalizer in [76]. Both the system order and the set of significant delays were presumed to be known in this work. As stated earlier, this knowledge may be approximated from Barker probes. The result is similar to a concurrent paper [64] which did not require such knowledge and which we summarize below. Details beyond this summary and experimental results can be found in [78].

8.4.2.3 Sparse Adaptive Equalization

We begin our presentation of sparse adaptive equalization by creating a framework for the sparse channel identification problem. To this end, we focus on the T_s-spaced, phase-compensated channel and ignore the common tap-phase trajectory. We will refer to Figure 8.13, which illustrates the estimation of a D-dimensional vector $\mathbf{h}$, using the known input scalar sequence $\{d_m\}$ and the observed output sequence $\{y_m\}$ satisfying

$$y_m = \mathbf{h}^H \mathbf{d}(m) + v_m,$$

where $\mathbf{d}(n)$ denotes D consecutive elements of the sequence $\{d_m\}$. To determine the best estimated output sequence of the form $\hat{y}_{k,n} = \hat{\mathbf{h}}(n)^H \mathbf{d}(k)$, $\forall\, k \leq n$, we shall consider the deterministic least squares criterion $C_n(\hat{\mathbf{h}})$,

$$C_n(\hat{\mathbf{h}}) = \sum_{k=0}^{n} \lambda^{n-k} |y_k - \hat{y}_{k,n}|^2. \tag{8.25}$$

As shown in Figure 8.13, we are interested in representing the channel estimate in a two-step process: through a $D_s \times D$ *selection matrix* $\mathbf{S}$ ($D_s < D$) and a D_s-dimensional vector $\hat{\mathbf{h}}_\mathbf{S}(n)$ such that $\hat{\mathbf{h}}(n) = \mathbf{S}^H \hat{\mathbf{h}}_\mathbf{S}(n)$. The matrix $\mathbf{S}$ is so named since its row vectors form a subsequence of D_s rows from the $D \times D$ identity matrix, $\mathbf{I}$. Note that $\mathbf{S}\mathbf{S}^H$

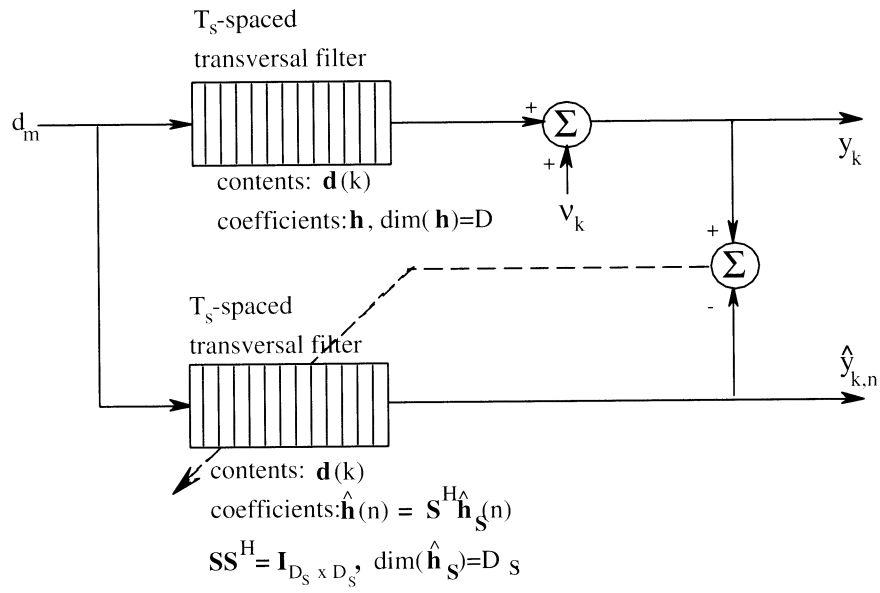

Figure 8.13 Sparse channel estimation.

is the $D_s \times D_s$ identity matrix, and that $\mathbf{S}$ allows the D_s components of $\hat{\mathbf{h}}_\mathbf{S}(n)$ to estimate a channel having a delay spread much greater than $T_s D_s$ seconds. We are interested in selecting D_s, $\mathbf{S}$, and $\hat{\mathbf{h}}_{\mathbf{S}(n)}$ at each time n to estimate the observation sequence y_k, $0 \le k \le n$ with an accuracy measured by $C_n(\hat{\mathbf{h}})$.

We begin with the special case of $\mathbf{S} = \mathbf{I}$ to develop the solution for $\hat{\mathbf{h}}_\mathbf{S}(n) = \hat{\mathbf{h}}_\mathbf{I}(n)$ and to relate this to the general case. When $\mathbf{S}$ is the identity matrix, the estimator $\hat{\mathbf{h}}_\mathbf{I}(n)$, which minimizes C_n, is found via weighted least squares regression,

$$\hat{\mathbf{h}}_\mathbf{I}(n) = \mathbf{R}_{dd}^{-1}(n)\mathbf{p}(n), \tag{8.26}$$

where

$$\begin{aligned} \mathbf{R}_{dd}(n) &= \lambda \mathbf{R}_{dd}(n-1) + \mathbf{d}(n)\mathbf{d}^H(n) \\ \mathbf{p}(n) &= \lambda \mathbf{p}(n-1) + y_n^* \mathbf{d}(n), \end{aligned} \tag{8.27}$$

with initial conditions $\mathbf{R}_{dd}(-1) = \mathbf{0}$, $\mathbf{p}(-1) = \mathbf{0}$. Note that both y_i and d_i, which are used to form the linear estimator, are available to the receiver via observation, training sequences, or accurately detected data. The minimal cost for $\mathbf{S} = \mathbf{I}$ is

$$C_n(\hat{\mathbf{h}}_\mathbf{I}) = R_{yy}(n) - \hat{\mathbf{h}}_\mathbf{I}^H(n)\mathbf{p}(n), \tag{8.28}$$

where $R_{yy}(n) = \sum_{k=0}^{n} \lambda^{n-k} y_k y_k^*$.

An update complexity of $O(D)$ for the series $\{\hat{\mathbf{h}}_{\mathbf{I}}(n)\}$ can be provided by an RLS-type algorithm. However, for a judicious choice of the selection matrix $\mathbf{S}$ and for sparse systems, the update complexity for the series $\{\mathbf{S}^H \hat{\mathbf{h}}_{\mathbf{S}}(n)\}$ can be lessened by an additional order of magnitude. The added cost $C_n(\mathbf{S}^H \hat{\mathbf{h}}_{\mathbf{S}}) - C_n(\hat{\mathbf{h}}_{\mathbf{I}})$ for this complexity decrease can also be precomputed. To see this, we quantify the accompanying increase in C_n when the estimator uses $\mathbf{S} \neq \mathbf{I}$, relative to the case $\mathbf{S} = \mathbf{I}$. For a fixed $\mathbf{S}$, the estimator $\hat{\mathbf{h}}_{\mathbf{S}}(n)$ that minimizes $C_n(\mathbf{S}^H \hat{\mathbf{h}}_{\mathbf{S}}(n))$ from (8.25) is

$$\hat{\mathbf{h}}_{\mathbf{S}}(n) = [\mathbf{S}\mathbf{R}_{dd}(n)\mathbf{S}^H]^{-1}\mathbf{S}\,\mathbf{p}(n). \tag{8.29}$$

Due to the selection matrix $\mathbf{S}$, the channel estimator is constrained to have a sparse structure. Since $\mathbf{S}\mathbf{R}_{dd}(n)\mathbf{S}^H$ and $\mathbf{S}\mathbf{p}(n)$ have similar recursions as for the case $\mathbf{S} = \mathbf{I}$, the RLS algorithms can be used to update $\mathbf{S}^H\hat{\mathbf{h}}_{\mathbf{S}}(n)$. Since the minimum cost associated with any selection matrix $\mathbf{S}$ is

$$C_n(\mathbf{S}^H \hat{\mathbf{h}}_{\mathbf{S}}) = R_{yy}(n) - \hat{\mathbf{h}}_{\mathbf{S}}^H(n)\mathbf{S}\mathbf{p}(n), \tag{8.30}$$

the incremental cost in reducing the estimator order to $D_s \leq D$ is

$$C_n(\mathbf{S}^H \hat{\mathbf{h}}_{\mathbf{S}}) - C_n(\hat{\mathbf{h}}_{\mathbf{I}}) = \mathbf{p}^H(n)[\mathbf{R}_{dd}^{-1} - \mathbf{S}^H(\mathbf{S}^H\mathbf{R}_{dd}(n)\mathbf{S})^{-1}\mathbf{S}]\mathbf{p}(n). \tag{8.31}$$

A critical step in an efficient sparsing algorithm is to find, in a simple fashion, the selection matrix $\mathbf{S}$ that minimizes D_s while satisfying a prescribed upper bound to the incremental cost given by the left-hand side of (8.31). Unfortunately, no simple rule exists for the general sparsing problem, and this fact will be shown to restrict the approach to sparse adaptive equalization. There are special cases of practical interest that permit efficient sparsing, however. For the case of *white* channel inputs, $E[\mathbf{R}_{dd}(n)] = a^2\mathbf{I}$, the incremental cost associated with the sparse estimator has strong intuitive appeal. In this case, the increase in squared error is

$$C_n(\mathbf{S}^H \hat{\mathbf{h}}_{\mathbf{S}}) - C_n(\hat{\mathbf{h}}_{\mathbf{I}}) = \frac{1}{a^2}\,\mathbf{p}^H(n)[\mathbf{I} - \mathbf{S}^H\mathbf{S}]\mathbf{p}(n). \tag{8.32}$$

For the case of white inputs, the incremental error is the total energy in the components of $\mathbf{p}(\mathbf{n})$ corresponding to the rows of $\mathbf{I}$ not taken to form $\mathbf{S}$. As seen from (8.27), the energy in a component of $\mathbf{p}(n)$ is proportional to the energy of the channel tap at that location, and $E[\mathbf{p}(n)] = \mathbf{h}$. If the true channel, $\mathbf{h}$, has negligible energy at the ignored taps, then the increased cost due to a substantially simpler estimator is also negligible.

The squared error $C_n(\cdot)$ is directly related to the performance of the equalizer. For this reason, a careful selection of $\mathbf{S}$ is needed to maximally reduce the computational burden throughout a data packet without increasing $C_n(\mathbf{S}^H \hat{\mathbf{h}}_{\mathbf{S}})$ beyond a prescribed limit. There are at least two ways in which to proceed. The first

approach, suggested in [66] and [79], uses the magnitude sequence output from the modem's Barker correlator as an MIP estimator. This estimator provides important information for sparse systems, such as the number of *tap groups* (a group is a set of adjacent, significant taps), their centroids and spans. Adjacent or nearly adjacent tap groups are usually combined so as to minimize the total number of groups in the response, g. This decomposition relates any sparse approximation to the superposition of g subsystems and suggests an application of the *fast modular* RLS algorithm [69], whose update complexity is $O(D_s g + g^2)$. Provided $D_s \ll D$ and the group count g is small, then $D_s g + g^2 \ll D$, and a fast modular RLS algorithm is significantly simpler than FTRLS.

The second approach does not require a priori knowledge of the input delay-spread function structure, and was suggested in [64]. In this case, it is assumed that a data packet consists of an initial training sequence followed by an information sequence, and that full-order channel estimation ($\mathbf{S} = \mathbf{I}$) occurs for a brief period at the beginning of the packet. Full-order estimation provides $C_n(\hat{\mathbf{h}}_\mathbf{I})$ and $\mathbf{p}(n)$, which are required for the selection of D_s, $\mathbf{S}$ and $\hat{\mathbf{h}}_\mathbf{S}$. Experimental results have shown that full-order estimation must be implemented for only a short period (about 2D symbols) at the beginning of the packet, usually within the training period. While this application of full-order channel estimation does preserve the peak processing load, it does not substantially affect the average computational burden. The average computational burden is determined strongly by the choice of $\mathbf{S}$.

We now address the connection between reduced-complexity channel identification and channel equalization. We focus in particular on fractionally spaced DFEs. Does an accurate, low-order channel estimate $\hat{\mathbf{h}}_s$, with $D_s \ll D$, guarantee a reduced number of computations for equalizer tap adjustment? Not in general, as can be seen by the condition for the extremal equalizer coefficients for a minimum-MSE DFE. For jointly stationary vectors $\mathbf{r}(n)$, $\mathbf{d}(n)$ and for a zero-mean, unit-variance white sequence $\{d_m\}$, the vectors $\mathbf{a}$, $\mathbf{b}$ must satisfy

$$\begin{bmatrix} \mathcal{R}_{\mathbf{rr}} & -\mathcal{R}_{\mathbf{rd}} \\ -\mathcal{R}_{\mathbf{rd}}^H & \mathcal{R}_{\mathbf{dd}} \end{bmatrix} \begin{bmatrix} \mathbf{a} \\ \mathbf{b} \end{bmatrix} = \begin{bmatrix} \mathbf{f} \\ \mathbf{0} \end{bmatrix}, \tag{8.33}$$

where

$$\mathcal{R}_{\mathbf{vw}} = E\left[\mathbf{v}(n)\mathbf{w}^H(n)\right]$$

$$\mathbf{f} = [h(N_1 T_s) \;\; h((N_1 - 1)T_s) \;\; \ldots \;\; h(-N_2 T_s)]^T.$$

The statistical cross-correlations take the form

$$[\mathcal{R}_{\mathbf{rd}}]_{ij} = h(jT + N_1 T_s - (i-1)T_s)$$

$$[\mathcal{R}_{\mathbf{rr}}]_{ij} = \sigma^2 \delta_{ij} + \sum_{\alpha} h(\alpha T) h^*(\alpha T + (j-i)T_s),$$

where σ^2 is the additive noise variance. While a sparse, fractionally spaced channel $\mathbf{h}$ yields a sparse form for $\mathbf{f}$ and $\mathcal{R}_{\mathbf{rd}}$, the reduction in complexity for the solution of $\mathbf{a}$ and $\mathbf{b}$ is not readily apparent. One approach proposed in [78] is to apply the channel sparsing matrix $\mathbf{S}$ to the feedforward coefficient vector $\mathbf{a}$. This method preserves the adaptive matched-filter property of the feedforward filter and reduces the complexity of the solution for the equalizer coefficients. Sparse equalization of this form has been shown to reduce the average computational complexity per update by more than an order of magnitude in shallow-water acoustic channels.

8.4.3 Multiuser Detection

One of the first applications of multiuser detection (see Chapters 2 and 3) to the UAC is described in [80] and [36]. Vertical channel transmission with negligible multipath was considered. An adaptive K-user detector was used to resolve the temporal overlap of at most K short packets in a common request channel for a dynamic time division multiple access (TDMA) system. This receiver structure was a soft-decision two-stage detector and was provided information about the signature waveforms from packet headers. Using soft decisions to reconstruct and suppress cochannel interference has been shown to decrease the symbol error rate for low thermal noise conditions [82]. The parameter K was much smaller than the modem population size, and the sensitivity of request-channel throughput with K was explored [81]. This receiver was implemented and tested at sea for $K = 2$.

Multiple access techniques for shallow-water networks usually do not include time and frequency division because of the frequency-selective fading, limited system bandwidth, and the increased difficulties with global time slotting associated with platform mobility, as discussed in Section 8.1. Code-division multiple access (CDMA) is the preferred method for resource sharing in this environment. Until the early 1990s, however, little work was available on multiuser detection in time-varying dispersive channels, other than a bank of independently operating RAKE filters. In [83], two multiuser detectors were presented for a fixed frequency-selective channel which removed the bit-error-rate floor (versus average SNR) of the conventional RAKE detector. The floor was attributed to dominating cochannel interference, which was compensated for by the multiuser receivers. Fully adaptive, single-sensor multiuser receivers tailored for the shallow-water acoustic channel were presented first in [84] and most recently in [85] and are summarized below.

Figure 8.14 presents a block diagram description of this detector, which we refer to as a *multiuser DFE*, or MDFE, and which can be compared with the multiuser DFE structures described in Chapters 3 and 4.

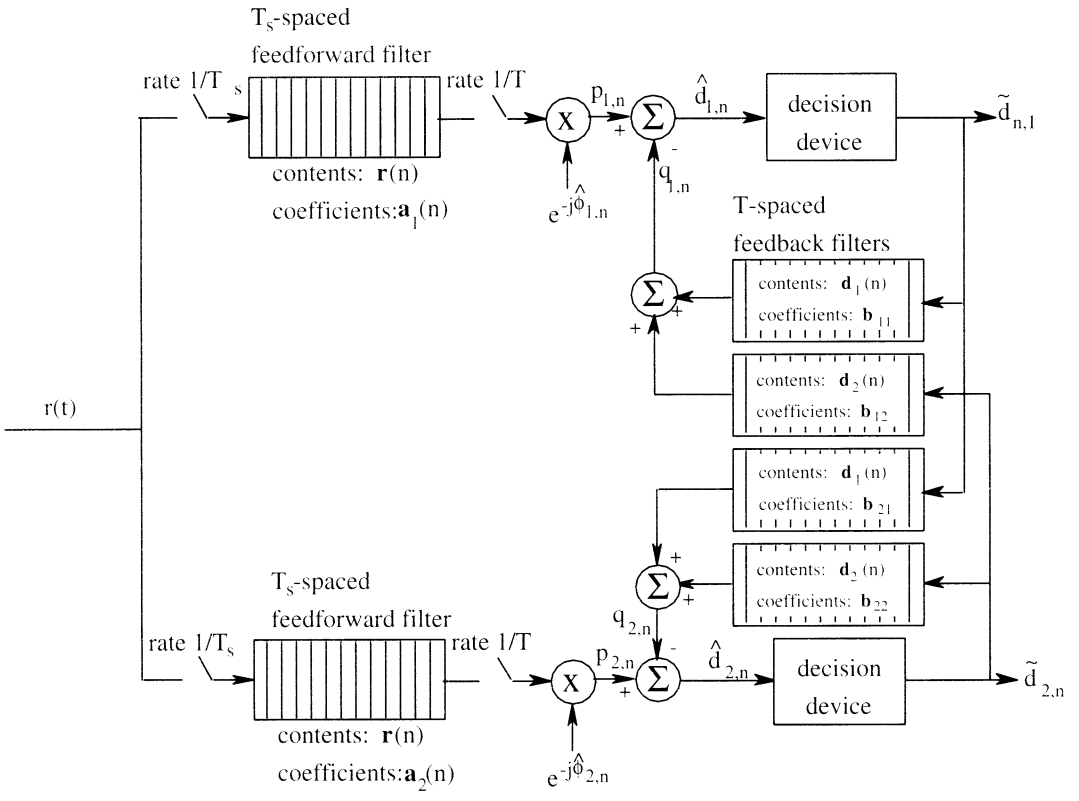

Figure 8.14 Multiuser decision feedback equalizer.

Note the strong similarity of this receiver to a bank of K conventional, fractionally spaced DFEs, with the exception of the "crossover" feedback filters $\mathbf{b}_{ji}$, $i \neq j$ in Figure 8.14. This single-sensor multiuser receiver consists of one fractionally spaced feedforward filter and K symbol-spaced feedback filters for each of the K users in the system. The sampled input signal in every feedforward section at time nT is given by

$$\mathbf{r}(n) = [r(nT + N_1T_s) \;\; r(nT + (N_1 - 1)T_s) \;\; \cdots \;\; r(nT - N_2T_s)]^T. \tag{8.34}$$

The scalar output of the feedforward transversal filter for the kth user at time nT is given by $\mathbf{a}_k^H\mathbf{r}(n)$, where the combining coefficients are

$$\mathbf{a}_k = [a_{k,-N_1} \;\; \cdots \;\; a_{k,N_2}]^T.$$

We also define the output of the kth phase correction circuit at time nT as $p_{k,n} = \mathbf{a}_k^H\mathbf{r}(n)e^{-j\hat{\phi}_{k,n}}$. Similarly, the symbol-rate feedback filter for the ith receiver containing decisions from user j has an output at time nT given by $\mathbf{b}_{ij}^H\mathbf{d}_j(n)$, where

$$\mathbf{d}_j(n) = [\tilde{d}_{j,n-1} \;\; \cdots \;\; \tilde{d}_{j,n-M}]^T$$

and

$$\mathbf{b}_{ij} = [b_{ij1} \quad \cdots \quad b_{ijM}]^T.$$

As suggested by the notation, $\tilde{d}_{k,n}$ denotes the final decision for the nth symbol for user k, $d_{k,n}$. The sum of all K feedback transversal filters for user j at time nT is denoted as $q_{j,n}$. For the two-user case, the MDFE receiver produces for user 1 the feedback aggregate $q_{1,n} = \mathbf{b}_{11}^H \mathbf{d}_1(n) + \mathbf{b}_{21}^H \mathbf{d}_2(n)$, while the corresponding feedback aggregate for the conventional DFE would be $q_{1,n} = \mathbf{b}_{11}^H \mathbf{d}_1(n)$.

As shown in Figure 8.14, the decision variable for user k at time n is $\hat{d}_{k,n} = p_{k,n} - q_{k,n}$. It is convenient to represent this variable as the inner product

$$\hat{d}_{k,n} = \mathbf{c}_k^H \mathbf{u}_k(n),$$

where

$$\mathbf{c}_1 = [\mathbf{a}_1^T - \mathbf{b}_{11}^T - \mathbf{b}_{21}^T]^T,$$

$$\mathbf{u}_1(n) = [\mathbf{y}_1^T(n)\mathbf{d}_2^T(n)]^T, \tag{8.35}$$

and

$$\mathbf{y}_1(n) = [\mathbf{r}^T(n)e^{-j\hat{\varphi}_{1,n}}\mathbf{d}_1^T(n)]^T.$$

Final decisions for the data $d_{k,n}$ are denoted as $\tilde{d}_1(n)$ and are given by quantization (slicing) of the decision variable. The performance metric is a weighted sum of squared errors $e_{k,n} = d_{k,n} - \hat{d}_{k,n}$ when the symbol is known by the receiver in a training mode and $e_{k,n} = \tilde{d}_{k,n} - \hat{d}_{k,n}$ in a decision-directed mode. The receiver parameters at time nT are adjusted to minimize the weighted squared error $\mathcal{E}(n) = \sum_{k=0}^{n} \lambda^{n-k}\{|e_{1,n}|^2 + |e_{2,n}|^2\}$. Defining the cross-correlation matrix between the column vector sequences $\mathbf{x}(n)$ and $\mathbf{w}(n)$ as $\mathbf{R}_{xw}(n) = \lambda \mathbf{R}_{xw}(n-1) + \mathbf{x}(n)\mathbf{w}^H(n)$, the receiver parameters $\{\mathbf{c}_{1,\text{opt}}, \hat{\varphi}_{1,n}\}$ for user 1 which minimize $\mathcal{E}(n)$ are given by

$$\mathbf{c}_{1,\text{opt}} = \mathbf{R}^{-1}_{\mathbf{u}_1,\mathbf{u}_1}(n)\mathbf{R}_{\mathbf{u}_1,\mathbf{b}_1}(n)$$

and

$$\frac{\delta \mathcal{E}(n)}{\delta \hat{\varphi}_{1,n}} = -2\,\text{Im}[p_{1,n}e_{1,n}^*] = 0.$$

Since $\mathbf{u}_1$ depends on $\hat{\varphi}_{1,n}$, and $e_{1,n}$ depends on $\mathbf{u}_1(n)$, an approximate and computationally efficient solution to these equations can be achieved through the decoupling approach discussed earlier.

In this section, we have reviewed an adaptive receiver structure for the MDFE for K asynchronous users. A bank of K conventional DFEs is a special case of this presentation and is given by the substitution of $\mathbf{y}_1(n)$ for $\mathbf{u}_1(n)$ in this section. In [85], the improvement due to the crossover filters $\mathbf{b}_{ij}$ is quantified. It is shown there that

$$E\{\mathcal{E}_{\text{MDFE}}\} \approx 1 - \mathcal{R}_{\mathbf{d}_1\mathbf{u}_1}\mathcal{R}^{-1}_{\mathbf{u}_1\mathbf{u}_1}\mathcal{R}_{\mathbf{u}_1\mathbf{d}_1},$$

$$E\{\mathcal{E}_{\text{DFE}}\} \approx 1 - \mathcal{R}_{\mathbf{d}_1\mathbf{y}_1}\mathcal{R}^{-1}_{\mathbf{y}_1\mathbf{y}_1}\mathcal{R}_{\mathbf{y}_1\mathbf{d}_1},$$

where $\mathcal{R}_{\mathbf{wx}}$ denotes a statistical cross-correlation matrix. These expressions are valid under the additional assumption that the data symbols $\{d_{k,n}\}$ are uncorrelated with zero mean and unit variance and can be used to show that the MDFE outperforms the DFE in a multiple-access setting [85]. The two detectors have comparable performance in the unusual case when $\mathbf{d}_2$ and $\mathbf{y}_1$ are statistically uncorrelated.

8.4.4 Wideband Array Signal Processing

As discussed in Chapters 1, 2, and 4, the use of a spatial arrays of receivers, which we refer to as multichannel receivers, can improve the demodulation capabilities of communications systems. If the receivers are widely separated so that the fluctuations in the channels from the transmitter to one receiver are independent of those to another receiver, explicit diversity techniques can be exploited to enable the overall system to overcome fading in one or more of the independent channels. If the fluctuations in the channels to different receivers are not independent, then the coherent spatial structure of the received signal can be exploited. One of two different approaches is usually taken in coherently combining the signals at the receivers. The first approach is to attempt to capture all of the signal energy that has propagated from the transmitter to the receivers. The second is to attenuate the signals that have propagated through some ray tubes while accentuating signals that have propagated through other ray tubes. The latter approach corresponds to traditional beamforming. In the multiuser environment, the multichannel receiver can use the differences in the spatial structure of the signals transmitted by different users to distinguish between interfering arrivals [16, 90].

We begin with the approach developed in [45], which is an extension of the adaptive single-channel equalizer discussed in Section 8.4.1 and shown in Figure 8.12. The single input channel is replaced by K input channels, K feedforward filters, and K PLLs. The input to the kth channel is $r_k(t)$, the coefficient vector of the kth feedforward filter is $\mathbf{a}_k(n)$, and the phase of the kth PLL is $\varphi_{n,k} = \omega_{d,n,k} n + \theta_{n,k}$. The outputs of the individual channels are summed to form

$$p_n = \sum_{k=1}^{K} \mathbf{a}_k^H(n)\mathbf{r}_k(n)e^{-j\varphi_{n,k}}. \tag{8.36}$$

The tap weight vector given by

$$\mathbf{u}(n) = \begin{bmatrix} \mathbf{a}_1(n) \\ \vdots \\ \mathbf{a}_K(n) \\ \mathbf{b}(n) \end{bmatrix} \tag{8.37}$$

is determined with a least squares metric, as in Section 8.4.1 for the single-channel equalizer. The optimal phase correction terms $\varphi_{n,1}$ through $\varphi_{n,K}$ are individually estimated using a second-order digital PLL.

The computational complexity required to compute the optimal tap weight vector grows with K^2, yielding an often unacceptable level of complexity. Approaches to reducing the complexity associated with multichannel algorithms in the underwater environment have been developed [16, 89]. Like the sparsing approach to complexity reduction described in Section 8.4.2, these multichannel algorithms achieve their complexity reduction by exploiting particular features of the propagation environment.

The approach in [89] is built around an essentially deterministic ray propagation model. Let P denote the number of rays from the transmitter to the receiver array, and assume that $P < K$. Then, assuming that the ray paths are known, it is shown that there is no loss in performance if a K-input, P-output beamformer is used to transform the outputs of the K sensors into P-channel signal, with the pth channel carrying the signal that propagated along the pth ray. This P-channel beamformer output is followed by a P-channel equalizer. A complexity reduction is realized in calculating the weights of the multichannel equalizer since the dimension of the receiver parameter vector $\mathbf{u}(n)$ is proportional to P. When the characteristics of the P ray paths are not known or are time varying, the front-end beamformer is required to adapt. The beamformer adaptation algorithm in [89] is based on three assumptions. The first is that the signals can be reasonably modeled as narrowband signals. The second is that the transmitter is far enough from the receiver array and the environment is sufficiently homogeneous that the propagating signal is a plane wave across the aperture of the array. The final assumption is that the array is linear with uniform spacing between sensors. When these assumptions are fulfilled, a memoryless beamformer with complex-valued, unit-norm weights is sufficient to achieve the desired signal separation and a relatively simple PLL algorithm can be used to calculate the needed beamformer weights. An ad hoc approach to updating the unconstrained weights of a memoryless beamformer is described for the case where the above assumptions are not valid.

The reduced complexity multichannel beamformers developed in [16] are based upon the micro-/macro-multipath propagation model developed in Section 8.1.4. The multichannel demodulator consists of a K input, single-output tapped-delay-line beamformer followed by a single-channel equalizer such as the one described in Section 8.4.1. This structure is based upon several assumptions. The first is that the intersensor correlation of the clusters of arrivals for the dominant ray tube is reasonably strong. The second assumption is that the macro-multipath provides sufficiently different spatial/temporal structure to signals that propagate through different ray tubes so that the front-end beamformer can distinguish between these

different signals by using only that structure. Given these assumptions, the front-end beamformer can eliminate most of the intersymbol interference from multipath arrivals from other than the dominant ray tube and the multiple-access interference from other transmitters without having to adapt to the fluctuations in the micro-multipath structure of the environment. Complexity reduction is achieved because the macro-multipath structure of the channel to which the beamformer must adapt changes fairly slowly and therefore the weights of the beamformer can be updated infrequently. This method of complexity reduction therefore belongs to the *reduced update* class of techniques described in Section 8.4.2. The single-channel output of the beamformer contains only a modest amount of intersymbol interference due to the micro-multipath spread of the dominant ray tube and a greatly reduced amount of multiple-access interference. A small single-channel equalizer is used to complete the demodulation process.

8.5 Concluding Remarks

In this chapter, we have presented a first-principles model for the UAC, and we have discussed many of the characteristics that distinguish this channel from the RF channels discussed in earlier chapters. Our model was developed using the concept of ray propagation through random nonhomogeneous media, by introducing the notion of ray tubes. The effect of environmental fluctuations on the communication channel were decomposed into macro- and micro-multipath input delay-spread functions. This model was used to relate channel saturation to the temporal and spatial coherence of the input delay-spread functions. We have focused on signal processing techniques for situations when the input delay-spread function exhibited a separable decomposition $g(t, \tau) \approx h(\tau)e^{j(\omega_d t+\theta)}$. This explicit modeling of the Doppler shift permits reliable phase-coherent demodulation in time-varying shallow-water UACs. We have presented techniques to reduce the computational complexity for both single-sensor and multisensor receivers; these techniques exploited features germane to the underwater channel. Multiuser detectors find a natural application in this channel and were presented in this chapter as extensions of the single-channel equalizers.

We have also presented current research on several open problems in phase-coherent communications through UACs. Current and future research topics include adaptive detection in multipath channels that exhibit path-dependent Doppler shifts, wideband coherent detection for severe Doppler dilation, and coherent demodulation algorithms with reduced computational complexity. We conclude this chapter with an extensive bibliography detailing past and recent work in the field.

REFERENCES

[1] T. G. Bell, "Sonar and Submarine Detection," *U.S. Navy Underwater Sound Lab. Rep.* 545, 1962.

[2] L. M. Brekhovskikh, Y. P. Lysonov, *Fundamentals of Ocean Acoustics*, 2nd Edition, Springer-Verlag, Berlin, 1991.

[3] C. S. Clay, H. Medwin, *Acoustical Oceanography: Principles and Applications*, John Wiley and Sons, New York, 1977.

[4] D. Kilfoyle, J. Catipovic, "Dynamic Viterbi Decoding in Underwater Acoustic Channels under Burst Noise Conditions," in *Proc. OCEANS'96*, Fort Lauderdale, FL, 1996, pp. 832–838.

[5] M. Buckingham, C. Epifanio, M. Readhead, "Passive Imaging of Targets with Ambient Noise: Experimental Results," *J. Acoust. Soc. Am.*, Vol. 100, No. 4, Pt. 2, October 1996, pp. 27–36.

[6] J. Bellingham, H. Schmidt, M. Deffenbaugh, "Acoustically Focused Oceanographic Sampling in the Haro Strait Experiment," *J. Acoust. Soc. Am.*, Vol. 100, No. 4, Pt. 2, October 1996, p. 2612.

[7] S. Flatte, ed., *Sound Transmission Through a Fluctuating Ocean*, Cambridge University Press, Cambridge, 1979.

[8] S. Flatte, "Wave Propagation Through Random Media: Contributions from Ocean Acoustics," *Proc. IEEE*, Vol. 71, No. 11, November 1983, pp. 1267–1294.

[9] T. Duda, S. Flatte, D. Creamer, "Modelling Meter-Scale Acoustic Intensity Fluctuations from Oceanic Fine Structure and Microstructure," *Journal of Geophysical Research*, Vol. 93, No. C5, May 1988, pp. 5130–5142.

[10] T. Duda, "Modeling Weak Fluctuations of Undersea Telemetry Signals," *IEEE J. Oceanic Eng.*, Vol. 16, No. 1, January 1991, pp. 3–11.

[11] L. Ziomek, "Generalized Kirchhoff Approach to the Ocean Surface Scatter Communication Channel. Part I. Transfer Function of the Ocean Surface," *J. Acoust. Soc. Am.*, Vol. 71, No. 1, January 1982, pp. 116–126.

[12] L. Ziomek, "Generalized Kirchhoff Approach to the Ocean Surface Scatter Communication Channel. Part II. Second-order Functions," *J. Acoust. Soc. Am.*, Vol. 71, No. 6, June 1982, pp. 1487–1495.

[13] D. Dowling, D. Jackson, "Coherence of Acoustic Scattering from a Dynamic Rough Surface," *J. Acoust. Soc. Am.*, Vol. 93, No. 6, June 1993, pp. 3149–3157.

[14] R. Owen, B. Smith, R. Coates, "An Experimental Study of Rough Surface Scattering and Its Effects on Communication Coherence," in *Proc. OCEANS'94*, Brest, France, Vol. III, 1994, pp. 483–488.

[15] H. Schmidt, Personal communications regarding results of 1996 Haro Strait experiment.

[16] S. Gray, J. Preisig, D. Brady, "Multi-user Detection in a Horizontal Underwater Acoustic Channel Using Array Observations," *IEEE Trans. Signal Process.* Special Issue on Signal Processing for Advanced Communications,Vol. 45, No. 1, January 1997, pp. 148–160.

[17] P. Bello, "Characterization of Randomly Time-Variant Linear Channels," *IEEE Trans. Commun. Systems*, CS-11, December 1963, pp. 360–393.

[18] D. Farmer, S. Clifford, J. Verral, "Scintillation Structure of a Turbulent Tidal Flow," *Journal of Geophysical Research*, Vol. 92, No. C5, May 1987, pp. 5369–5382.

[19] T. Eggen, "Underwater Acoustic Communications over Doppler Spread Channels," Ph.D. Thesis, Massachusetts Institute of Technology and Woods Hole Oceanographic Institution, Cambridge, MA, June 1997.

[20] B. Woodward, H. Sari, "Digital Underwater Acoustic Voice Communications," *IEEE J. Oceanic Eng.*, Vol. 21, No. 2, April, 1996, pp. 181–192.

[21] H. O. Berktay, B. Gasey, and C. A. Teer, "Underwater Communication: Past, Present and Future," *J. Sound Vib.*, Vol. 7, pp. 62–70, 1968.

[22] A. Baggeroer, "Acoustic Telemetry—An Overview," *IEEE J. Oceanic Eng.*, Vol. 9, No. 4, October, 1984, pp. 229–235.

[23] M. Stojanovic, "Recent Advances in High-Speed Underwater Acoustic Communications," *IEEE J. Oceanic Eng.*, Vol. 21, No. 2, April, 1996 pp. 125–136.

[24] *IEEE J. Oceanic Eng.* Special issue on Ocean Acoustic Data Telemetry, Vol. 16, No. 1, January, 1991, pp. 1–177.

[25] J. A. Catipovic, *Design and Performance Analysis of a Digital Acoustic Telemetry System*, Doctoral Dissertation, Woods Hole Oceanographic Institution/MIT, May, 1988.

[26] A. Clark, "Diver Communications—The Case for Single Sideband," *Underwater System Design*, 1989, pp. 16–18.

[27] W. Dow, "A Telemetering Hydrophone," *Deep-Sea Research*, Vol. 7, 1960, pp. 142–147.

[28] P. Hearn, "Underwater Acoustic Telemetry," *IEEE Trans. Commun. Tech.*, Vol. CT-14, Dec. 1966, pp. 839–843.

[29] G. M. Walsh, A. P. Alair, A. S. Westneat, "Establishing Reliability and Security in an Offshore Command Link," *Proc. Offshore Tech. Conference*, 1969.

[30] F. R. Mackelburg, S. J. Watson, A. Gordon, "Benthic 4800 bits/second Acoustic Telemetry," *Proc. OCEANS, 1981*, p. 78.

[31] J. G. Proakis, *Digital Communications*, 3rd edition, New York, McGraw-Hill, 1995.

[32] R. Price, P. E. Green, Jr., "A Communication Technique for Multipath Channels," *Proc. IRE*, Vol. 46, March, 1958, pp. 555–570.

[33] P. Monsen, "Theoretical and Measured Performance of a DFE Modem on a Fading Multipath Channel," *IEEE Trans. Commun.*, Vol. COM-25, Oct. 1977, pp. 1144–1153.

[34] J. Catipovic, A. B. Baggeroer, K. Von Der Heydt, D. Koelsch, "Design and Performance Analysis of Digital Acoustic Telemetry Systems for the Short Range Underwater Channel," *IEEE J. Oceanic Eng.*, Vol. OE-9, No. 4, October, 1984, pp. 242–252.

[35] S. Coatelan, A. Glavieux, "Design and Test of a Multicarrier Transmission System on the Shallow Water Acoustic Channel," *Proc. OCEANS '94*, Brest, France, Vol. 3, 1994, pp. 472–477.

[36] D. Brady, J. Catipovic, "Adaptive Multiuser Detection for Underwater Acoustic Channels," *IEEE J. Oceanic Eng.*, Vol. 19, April 1994, pp. 158–165.

[37] http://www.datasonics.com/products/modems/atm850.htm

[38] J. Catipovic, "Performance Limitations in Underwater Acoustic Telemetry," *IEEE J. Oceanic Eng.*, Vol. 15, July, 1993, pp. 205–216.

[39] R. Galvin, R. F. W. Coates, "Analysis of the Performance of an Underwater Acoustic Communication System and Comparison with a Stochastic Model," in *Proc. OCEANS'94*, Brest, France, 1994, pp. 478–482.

[40] A. Essebbar, F. Loubet, F. Vial, "Underwater Acoustic Channel Simulations for Communication," in *Proc. OCEANS'94*, Brest, France, 1994, pp. 495–500.

[41] S. J. Roberts, "An Echo Canceller Technique Applied to an Underwater Acoustic Data Link," Ph.D. Thesis, Department of Electrical and Electronic Engineering, Herriot Watt University, Edinburgh, Scotland, September, 1983.

[42] G. Sandsmark, *The Feasibility of Adaptive Equalization in High Speed Underwater Acoustic Data Transmission*, Ph.D. thesis, NTH, Trondheim, Norway, 1990.

[43] J. Catipovic, M. Deffenbaugh, L. Freitag, D. Frye, "An Acoustic Telemetry System for Deep Ocean Mooring Data Acquisition and Control," *Proc. OCEANS'89*, Seattle, WA, 1989, pp. 887–892.

[44] M. Stojanovic, J. Catipovic, J. G. Proakis, "Phase-Coherent Digital Communications for Underwater Acoustic Channels," *IEEE J. Oceanic Eng.*, Vol. 19, No. 1, January, 1994, pp. 100–111.

[45] M. Stojanovic, J. Catipovic, and J. Proakis, "Adaptive Multichannel Combining and Equalization for Underwater Acoustic Communications," *J. Acoust. Soc. Am.*, Vol. 94, No. 3, Pt. 1, Sept. 1993, pp. 1621–1631.

[46] D. Falconer, "Jointly Adaptive Equalization and Carrier Phase Recovery in Two Dimensional Digital Communication Systems," *Bell Syst. Techn. J.*, Vol. 55, March, 1976, pp. 317–334.

[47] R. Coates, "Underwater Acoustic Communications," *Proc. OCEANS'93*, Victoria, BC, Canada, Vol. 3, October, 1993, pp. 420–425.

[48] R. Gitlin, S. Weinstein, "Fractionally Spaced Equalization: An Improved Digital Transversal Equalizer," *Bell Syst. Techn. J.*, Vol. 60, Feb. 1981, pp. 275–296.

[49] D. T. M. Slock, T. Kailath, "Fast Transversal RLS Algorithms," in *Adaptive System Identification and Signal Processing Algorithms*, N. Kalouptsidis, S. Theodoridis, Editors, Englewood Cliffs, NJ: Prentice Hall, 1993, pp. 123–190.

[50] D. T. M. Slock, T. Kailath, "Numerically Stable Fast Transversal Filters for Recursive Least Squares Adaptive Filtering," *IEEE Trans. Signal Process.*, Vol. 39, Jan., 1991, pp. 92–114.

[51] M. Johnson, L. Freitag, M. Stojanovic, "Improved Doppler Tracking and Correction for Underwater Acoustic Communications," *Proc. ICASSP, 1996* Atlanta, Ga., Vol. 1, pp. 575–578.

[52] B. Geller, V. Capellano, J.-M. Brossier, A. Essebbar, G. Jourdain, "Equalizer for Video Rate Transmission in Multipath Underwater Communications," *IEEE J. Oceanic Eng.*, Vol. 21, No. 2, April, 1996, pp. 150–155.

[53] A. Kaya, S. Yauchi, "An Acoustic Communication System for Subsea Robot," *Proc. OCEANS'89*, Seattle, WA, Oct. 1989, pp. 765–770.

[54] M. Suzuki, T. Sasaki, "Digital Acoustic Image Transmission System for Deep Sea Research Submersible," *Proc. OCEANS'92*, Newport, RI, Oct. 1992, pp. 567–570.

[55] A. Benveniste, M. Metivier, P. Priouret, *Adaptive Algorithms and Stochastic Approximations*, New York: Springer-Verlag, 1990.

[56] W. A. Sethares, "The Least Mean Square Family," in *Adaptive System Identification and Signal Processing Algorithms*, N. Kalouptsidis and S. Theodoridis, editors, Englewood Cliffs, NJ: Prentice Hall, 1993, pp. 84–122.

[57] L. Barbosa, "Maximum Likelihood Sequence Estimators: A Geometric View," *IEEE Trans. Inform. Theory*, Vol. 35, No. 2, March 1989, pp. 419–427.

[58] D. Divsalar, "Performance of Mismatched Receivers on Bandlimited Channels," Ph.D. thesis, UCLA, 1978.

[59] J. Habermann, D. Dzung, "Performance of Coherent Data Transmission with Imperfect Channel Estimation in Frequency-Selective Rayleigh Fading Channels: Cochannel and Adjacent Channel Interference," *AEU*, Vol. 44, No. 5, Sept./Oct., 1990, pp. 1680–1686.

[60] F. Gozzo, "Robust Sequence Estimation in the Presence of Channel Mismatch," *IBM Federal Systems Report 92-OTP-050.*

[61] M. Stojanovic, J. Proakis, J. Catipovic, "Analysis of the Impact of Channel Estimation Errors on the Performance of a Decision-Feedback Equalizer in Fading Multipath Channels," *IEEE Trans. Commun.*, Vol. 43, Feb./Mar./Apr., 1995, pp. 877–886.

[62] S. Fechtel, H. Meyr, "An Investigation of Channel Estimation and Equalization Techniques for Moderately Rapid Fading HF-Channels," *Proc. ICC'91*, Denver, CO, 1991, pp. 768–772.

[63] P. D. Shukla, L. F. Turner, "Channel-Estimation-Based Adaptive DFE for Fading Multipath Radio Channels," *IEE Proceedings, Part I*, Vol. 138, No. 6, Dec. 1991, pp. 525–543.

[64] M. Kocic, D. Brady, "Complexity-Constrained RLS Algorithm for Sparse Channels," *Proc. Conf. Inform. Science Sys.'94*, Princeton, NJ, March, 1994, pp. 420–425.

[65] M. Kocic, D. Brady, M. Stojanovic, "Sparse Equalization for Real-Time Digital Underwater Acoustic Communications," *Proc. OCEANS'95*, San Diego, CA, 1995, pp. 1417–1422.

[66] L. Freitag, M. Johnson, "A Robust and Efficient Receiver for Coherent Acoustic Communications," submitted to *IEEE J. Oceanic Eng.*, 1997.

[67] *Haro Straits data* at http://telem.whoi.edu/.

[68] P. Anderson, "Adaptive Forgetting in Recursive Identification Through Multiple Models," *Int. J. Control*, 42(5), 1984, pp. 1175–1193.

[69] D. Slock, L. Chisci, H. Lev-Ari, T. Kailath, "Modular and Numerically Stable Fast Transversal Filters for Multichannel and Multiexperiment RLS," *IEEE Tran. Acoust. Speech Sig. Process.*, vol. ASSP-40, April 1992, pp. 784–802.

[70] Y. F. Cheng and D. M. Etter, "Analysis of an Adaptive Technique for Modeling Sparse Systems," *IEEE Trans. Acoust. Speech Sig. Process.*, Vol. ASSP-37, No. 2, Feb. 1989, pp. 254–264.

[71] D. Wilson, "Optimum Solution of Model-Reduction Problem," *Proc. IEE*, Vol. 117, No. 6, June 1970, pp. 1161–1165.

[72] K. Nagpal, R. Hemlick, C. Sims, "Reduced-order Estimation: Part 1. Filtering," *International Journal of Control*, Vol. 45, No. 6, 1987, pp. 1867–1888.

[73] B. Moore, "Principal Component Analysis in Linear Systems: Controllability, Observability and Model Reduction," *IEEE Trans. Autom. Control*, Vol. AC-26, No. 1, February 1981, pp. 17–32.

[74] H. Kim, C. Sims, K. Nagpal, "Reduced Order Filtering in H-Infinity Setting," *Proceedings of American Control Conference*, 1992, pp. 1876–1877.

[75] N. Siddiqui, C. Sims: "Filter Order Reduction Using Mean Value and Covariance Matching Technique," *Proceedings of American Control Conference*, 1992, pp. 1789–1793.

[76] D. Reynolds, C. Sims, L. Tong, "Adaptive Equalization of a Digital Communications Channel with a Reduced-Order Equalizer," *Proc. 1994 Asilomar Conf*, Monterey, CA, November 1994, pp. 1428–1432.

[77] B. Geller, V. Capellano, J. M. Brossier, "Equalizer for High Data Rate Underwater Communications," *Proc. OCEANS'94*, Brest, France, 1994.

[78] M. Kocic, D. Brady, M. Stojanovic, "Reduced Complexity Equalization for Acoustic Telemetry in Shallow Water," submitted to *IEEE J. Oceanic Eng.*

[79] M. Johnson, D. Brady, M. Grund, "Reducing the Computational Requirements of Adaptive Equalization in Underwater Acoustic Communications," *Proc. OCEAN'95*, San Diego, CA, Vol. 3, 1995, pp. 1405–1410.

[80] D. Brady, J. Catipovic, "Adaptive Soft-Decision Multiuser Receiver for Underwater Acoustical Channels," *Proc. 1992 Asilomar Conf.*, Pacific Grove, CA, Vol. 2, Oct. 1992, pp. 1137–1141.

[81] D. Brady, L. Merakos, "Throughput Performance of Multiuser Detection in Unslotted Contention Channels," *Proc. INFOCOM,* Toronto, Canada, Vol. 2, June, 1994, pp. 610–617.

[82] X. Zhang, D. Brady, "Asymptotic Multiuser Efficiencies for Decision-Directed Multiuser Detectors," *IEEE Trans. Info. Theory*, Vol. 44, No. 2, March 1998, pp. 502–515.

[83] Z. Zvonar, D. Brady, "Coherent and Differentially Coherent Multiuser Detectors for Asynchronous CDMA Frequency-Selective Channels," *Proc. MILCOM, 1992*, pp. 17.6.1–17.6.5.

[84] Z. Zvonar, D. Brady, "Adaptive Multiuser Receiver for Fading CDMA Channels With Severe ISI," *Proc. Conf. Inform. Sc. Sys., 1993*, pp. 324–329.

[85] Z. Zvonar, D. Brady, J. Catipovic, "Adaptive Detection for Shallow-Water Acoustic Telemetry with Cochannel Interference," *IEEE Trans. Oceanic Eng.*, Vol. 21, No. 4, 1996, pp. 528–536.

[86] J. Catipovic, L. Freitag, "Spatial Diversity Processing for Underwater Acoustic Telemetry," *IEEE J. Oceanic Eng.*, Vol. OE-15, 1991, pp. 205–216.

[87] Q. Wen, J. Ritcey, "Spatial Equalization for Underwater Acoustic Communications," in *Proc. 22nd Asilomar Conference on Signals, Systems and Computers*, 1992, pp. 1132–1136.

[88] O. Hinton, G. Howe, A. Adams, "An Adaptive, High Bit Rate, Sub-sea Communications System," in *Proc. of the European Conference on Underwater Acoustics,* Brussels, Belgium, editor, M. Weydert, Amsterdam, Elsevier Applied Science, 1992, pp. 75–79.

[89] M. Stojanovic, J. Catipovic, J. Proakis, "Reduced-complexity Spatial and Temporal Processing of Underwater Acoustic Communication Signals," *J. Acoust. Soc. Am.*, Vol. 98, No. 2, Pt. 1, August 1995, pp. 961–972.

[90] M. Stojanovic, Z. Zvonar, "Multichannel Processing of Broad-Band Multiuser Communication Signals in Shallow Water Acoustic Channels," *IEEE J. Oceanic Eng.*, Vol. OE-21, 1996, pp. 156–166.

ACKNOWLEDGMENT

This work was supported by Grant N0014-95-1-1316 from the Office of Naval Research.